Lateral Diffusion in the Ionic Liquid $[C_2Mim]^+[NTf_2]^-$ on Vacuum and Hydroxylated Sapphire Interfaces

Bachelorarbeit aus der Materialphysik

Vorgelegt von

Mario Udo Gaimann

am 27. September 2018

Physics Underlying Life Sciences Group

Institut für Theoretische Physik I

Friedrich-Alexander-Universität Erlangen-Nürnberg

Betreuerin: Prof. Dr. Ana-Sunčana Smith

Contents

List of Abbreviations

MD	Molecular Dynamics
MSD	Mean Squared Displacement
SLV	Solid – Liquid – Vacuum
VLV	Vacuum – Liquid – Vacuum

1 Introduction

Ionic liquids are a novel class of materials defined as molten salts being in the liquid state of matter below temperatures of 100 °C. They comprise of weakly interacting cations and anions, yielding a highly polar liquid [1]. Compared to conventional, single-atom ions such as sodium and chloride in everyday rock salt, the components of an ionic liquid are considerably bulky, charged molecules. While it seemed that the ability of ions to form an ionic liquid is a rare trait, a whole range of new materials was discovered in the last decades. Hereby, the choice of ions influences the structure of the liquid, which in turn determines its chemical and physical properties. Through combining suitable cations and anions, a tailored ionic liquid optimized for a specific application may be obtained [2], which is only one of many reasons why ionic liquids are of particular interest for current chemical research and industries. Hereby, room temperature ionic liquids are considered to be particularly promising due to their application potential [3].

The first desirable property is that ionic liquids can serve as a reaction medium free of protons, water or oxygen [4], acting as a solvent for organic, organometallic, and inorganic materials [5]. This enables a broad variety of chemical reactions [1, 6], yielding similar or improved functionality compared to conventional organic solvents [7]. Albeit being slightly sensitive to moisture through absorption, ionic liquids possess more desirable properties relating to chemical reactions: They bear a broad temperature range in which they are in a liquid state of matter, may exhibit several types of acidity, are inexpensive and may be readily obtained [8]. Their generally negligible vapour pressure allows for usage in high-vacuum systems and eased distillative separation of reaction products from the ionic liquid [6]. Consequently, both the ionic liquid as solvent and the catalyst may be reused multiple times, contributing to environmentally protective “green syntheses” practises.

In addition to ionic liquids functioning as solvents, these mixtures possess a broad electrical potential range in which neither reduction nor oxidization occurs, the so-called electrochemical window [9]. Together with general physical properties of high ionic conductivities, low viscosities [10] and a broad feasible temperature range [3], ionic liquids may be employed as electrolytes in batteries [11] as well as photoelectrical and electrochemical devices [12, 13]. Ionic liquids are further non-flammable, non-toxic and non-aggressive to metals [3], which would enhance the safety of potential products and scope of usage. Just to give some examples demonstrating the

versatility of these materials in terms of potential applications, ionic liquids may be employed in solar cells [14], fuel cells [15], batteries [16, 17], sensors [18] or electro-actuators for artificial muscles [19].

In order to utilize the outstanding properties of these materials, ionic liquids are often required to be in the vicinity to interfaces. electrolyte-electrode systems, ions of the opposite charge called *counter-ions*, assemble close to the interface and orient in the electric field, due to electrostatic interactions. In this way, electrical double layers are formed, which were first described by Helmholtz [20, 21] as fixed layers. Guoy and Chapman later extended the model by taking into account that particles immersed in a thermal environment are subject to Brownian motion, leading to a description incorporating diffusivity of ions [22]. However, neither description suffices to describe the complex nature of ionic liquids [23]. They are dominated by strong, long-range Coulomb interactions, which is why they are also referred to as dense room temperature ionic plasma or *Coulombic fluids* [24] and – most interestingly – all ionic liquids form layered or chequerboard structures in the vicinity of planar electrodes [25]. At neutral interfaces, such as ionic liquids close to a hydroxylated sapphire slab, hydrogen bonds between ions and the solid govern the interfacial structuring. This behaviour lead to the development of a new subclass of materials, such as *supported ionic liquid phase (SILP)* [26] and *solid catalysts with ionic liquid layer (SCILL)* [27] materials, enabling novel heterogeneous catalysis processes [28]. When looking closely at such a system in steady state, it is found that single ions exhibit Brownian motion, while the overall density distribution does not change with time. Those random movements are the foundation for diffusive behaviour, which itself relates to relevant physical quantities for applications such as viscosity. Computing diffusivities requires the precise spatial and temporal tracking of multiple ions. To achieve this *in silico*, the simulation technique of *molecular dynamics* has proven to adequately generate trajectories of ionic liquids[29] and also in cases where they are subject to interactions with interfaces [30].

There is consensus in the ionic liquid community, that a deep understanding of the surface and interface ordering of ionic liquids is crucial, in particular for future applications where electric layers plays a role [23, 28]. Motivated by this need for more basic research in this field, my thesis aims to contribute to the understanding of lateral self-diffusion in ionic liquids at solid–liquid and liquid–vacuum interfaces.

It is structured as follows: Firstly, the computational simulation technique of molecular dynamics will be addressed, followed by a review of conventional isotropic diffusion in bulk systems and anisotropic diffusion typically found in confined systems. Secondly, four systems will be introduced, namely reference systems of pure water and pure ionic liquid for method validation as well as vacuum–liquid–vacuum (VLV) and a solid–liquid–vacuum (SLV) systems. Thirdly, the trajectory processing methods and algorithms for the computation of diffusion coefficients and residence times will be outlined. And lastly, the resulting computed quantities for lateral diffusion, with reference to the x-y planes of systems, are presented and discussed.

2 Theory

2.1 Molecular Dynamics Simulations

Molecular dynamics (MD) simulations are a powerful computational tool, able to treat diverse sets of problems, ranging from protein folding in biology to interactions at charged surfaces in physics. Based on classical mechanics, the core principle of MD is solving Newton's equations of motion numerically. As a result, positions and velocities of the involved point particles can be computed for discrete time steps. And this is exactly where the power of MD lies: For every particle in the system, locations are known for every single time step, meaning that the evolution of a system can be fully comprehended. Computationally, this can be done efficiently by assuming all molecules being in their ground state, reducing atoms to point masses or even to "united atoms" in case of aliphatic carbon–hydrogen groups, for instance, and lastly applying the Born-Oppenheimer approximation [31].
However, the most important numerical concept here is describing the potential energy landscape for each particle using an effective interaction potential, a *force field*. It consists of multiple contributions, which can be separated into two groups, *bonded* interactions and *non-bonded* interactions [31]. The most prominent bonded interaction covers covalent bonds using a harmonic or Morse potential. If these interactions are particularly stiff, they may be fixed by implementing them as constrained bond lengths [31].
In contrast, non-bonded, short-range Pauli repulsions and long-ranged van der Waals attractions depend on the distance from one atom to another. They can be modelled using Lennard-Jones potentials, and are usually considered up to a certain cut-off radius around each atom. Charged contributions may be treated using Coulomb potentials. Considering polarizable molecules is computationally more expensive, which is why only one charge per atom is assumed in so-called *fixed-charge* force fields.
Most importantly, atomic interactions deterministically rely on the combination of these forces. As a consequence, choosing right parameters for a selected field is crucial for predicting physically correct particle behaviour. With the help of experiments, the parameters can be determined empirically. One may need to consider different kinds of force fields, for example in the case of cations and anions in ionic liquids. If two or more force fields encounter, for instance at solid–liquid interfaces, one must combine those fields according to specific rules. There are various such

combining rules known, such as geometric [32] or Lorentz-Berthelot [30] rules, and their choice might as well impact the outcome of an MD simulation. With these methods, one is now able to simulate the kinematic behaviour of particles in a thermal bath, which is described in the following section.

2.2 Brownian Motion and Isotropic Diffusion

At microscopic scales, motions of particles are – in contrast to objects in our macroscopic world – strongly influenced by thermal fluctuations. Their order of magnitude relates to the mean kinetic energy of a particle in three dimensions, being $3/2\, k_B T$, where k_B is the Boltzmann constant and T the temperature. As a consequence, any particle exhibiting directed motion gets highly distorted by random kicks from neighbouring particles in the same thermal bath. It ends up executing a *random walk* eventually, which is, notably, valid for particles of any size in general [33]. This effect was observed experimentally for pollen particles in water by Scottish botanist Robert Brown in 1827 [34]. Accordingly, particles subject to such thermally induced random walk were named *Brownian particles*, and their kinematic behaviour *Brownian motion*.
In this context, the spread of one or more Brownian particles into its surrounding substance due to thermal fluctuations is defined as *diffusion* [35]. From this microscopical perspective, diffusive behaviour indeed originates from random walks of individual particles [36, 37]. Nevertheless, it should be mentioned that diffusion may be derived phenomenologically using concentration gradients from a macroscopic point of view. For the equilibrated systems investigated in this thesis, however, no major changes in concentration are observed, and therefore one needs to speak of diffusion in a microscopic sense. Brownian motion of particles making up a liquid themselves leads in this regime to *self-diffusion* of those particles. For this reason, when speaking about diffusion in the following, actually self-diffusion is meant.

Let us now model a Brownian particle with velocity $\mathbf{v}$ as part of a liquid, in order to determine its thermally induced random transport properties. The particle with mass m is modelled by forming an equation of motion, incorporating a random force $\xi(t)$, dependent on time t, as well as a friction force with friction coefficient γ, giving

the *Langevin equation*

$$m\,\frac{\mathrm{d}\mathbf{v}(t)}{\mathrm{d}t} = -\gamma\mathbf{v}(t) + \xi(t)\,. \tag{1}$$

The random force contributions amount to zero when averaged over time, and there are no correlations between arbitrary times t and t'. It can be shown [38], that the Langevin equation mathematically equals a *Fokker-Planck equation*

$$\frac{\partial p(\mathbf{r},t)}{\partial t} = \nabla\cdot\left(-\mathbf{b}(\mathbf{r})\,p(\mathbf{r},t) + \nabla\cdot\left[\mathbf{D}(\mathbf{r},t)\,p(\mathbf{r},t)\right]\right)\,. \tag{2}$$

Here, $p(\mathbf{r},t)$ is the transition probability density dependent on a random variable, which is in this case its spatial coordinate $\mathbf{r} = (x,y,z)^\intercal$, and time t. The initial condition $p(\mathbf{r},0) = \rho_0(\mathbf{r})$ is assumed, where $\rho_0(\mathbf{r})$ is any initial probability density function [38]. The equation further includes $\mathbf{b}(\mathbf{r})$ as space-dependent drift vector, causing a shift of the probability density, and $\mathbf{D}(\mathbf{r},t)$ as diffusion tensor with entries

$$\mathbf{D}(\mathbf{r},t) = \begin{pmatrix} D_{xx} & D_{xy} & D_{xz} \\ D_{yx} & D_{yy} & D_{yz} \\ D_{zx} & D_{zy} & D_{zz} \end{pmatrix}\,. \tag{3}$$

This tensor has in the most general case both spatial and temporal dependencies. Diagonal entries correspond to independent diffusion in the directions given by the chosen coordinate system, while non-diagonal entries represent correlations of diffusivities in these directions.

Reducing Eq. 2 to one dimension by replacing the diffusion tensor $\mathbf{D}$ with a scalar D, assuming no drift $\mathbf{b}$ and constant diffusion, we find the *diffusion equation*

$$\frac{\partial}{\partial t}\,p(x,t) = D\frac{\partial^2}{\partial x^2}\,p(x,t)\,, \tag{4}$$

also known as *Fick's second law*. The proportionality constant D shall be called *diffusion coefficient* and fully characterizes the thermally induced random transport in one dimension. Eq. 4 can also be derived macroscopically from the continuity equation applied to Fick's phenomenological first law using concentrations instead of probability distributions [39], or from thermodynamics, as demonstrated by Einstein [33].

Let us now assume the initial probability density distribution $p(x_0, t_0)$ of a single particle is a delta distribution $\delta(x - x_0)$, and the density vanishes for $x \to \infty$ for all times. Applying these boundary conditions and setting $x_0, t_0 = 0$, one finds the special solution

$$p(x,t) = \frac{1}{\sqrt{4\pi D t}} \exp\left(-\frac{x^2}{4Dt}\right) . \tag{5}$$

Eq. 5 demonstrates the dynamics of the diffusion equation in one dimension. It can be visualised as a "melting" Gaussian distribution, with D determining the speed of this process. As such, the probability to find a particle at its initial location decreases with progressing time, and the probability to be located at a point far away from its initial location increases. Therefore, the spatial spread of a single particle with time is indeed described by a Gaussian function with mean $\langle x \rangle = 0$. However, the expectation value of $\langle x^2 \rangle$ is not zero. This value can be computed using the so-called *law of the unconscious statistician* [40], yielding [33, 39]

$$\left\langle x^2 \right\rangle = \int_{-\infty}^{\infty} x^2 \, p(x,t) \, \mathrm{d}x = 2Dt \, . \tag{6}$$

This is also known as *Einstein's diffusion relation*, stating that the average squared deviation of a particle's position is proportional to its displacement time, one of the key theorems of this thesis.

In this context it must be underlined, that the behaviour of particles strongly depends on the time scale. For small times compared to collision times, a particle will show ballistic behaviour, as it moves freely. Eventually, it may randomly collide with other particles and, as a consequence, undergo a random walk. Because of this, the sought after self-diffusion coefficient is given under the condition $t \to \infty$.

Lastly, Eq. 6 can be generalized for d Dimensions [37]. The diffusion coefficient in homogeneous liquids is therefore given by the expectation value of x^2 in three dimensions, being the mean squared displacement $\left\langle (\mathbf{\Delta r})^2 \right\rangle$ of N particles using $\mathbf{\Delta r} = (x - x_0, y - y_0, z - z_0)^\intercal$, as

$$D(t) = \lim_{t \to \infty} \frac{1}{d} \frac{\left\langle (\mathbf{\Delta r})^2 \right\rangle_N}{2t} \, . \tag{7}$$

Let us now consider an inhomogeneous system with a varying density profile. Trying to apply Eq. 7 in order to compute D for a strictly confined region of interest, for instance close to an interface, one ends up in a dilemma. The mean squared

displacement (MSD) will show linear behaviour only for long enough times. But then, particles may leave the region of interest and sample other regions, as schematically shown in Fig. 1a, yielding varying contributions to the MSD in dependence of their position. Therefore, a mere average for D over all considered regions can be obtained, but no precise value for the region of interest [32].

In this situation, one could restrain particle movements by introducing artificial, or virtual, absorbing boundaries. This would confine particles to specific regions. Once they crossed a boundary and left the region of interest, they would not contribute any more to this region. However, restraining particle movements implies curtailing the tails of probability density distributions which may lie in adjacent regions. This can be visualised as losing a vital part of the Gaussian distribution described in Eq. 5 at boundary positions, as sketched in Fig. 1b. As a result, particles with a large spatial deviation are neglected, and hence one systematically underestimates D. Note that the maximum value of the MSD in the direction being confined is then necessarily given by the squared width of the confined region.

On top of these considerations, Einstein's diffusion law does not hold generally for systems with non-uniform density distributions. The anisotropic Smoluchowski equation is required in this case, which will be presented in the following paragraph.

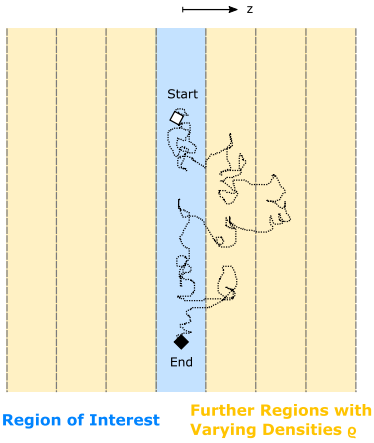

(a) 2D projection of a sample trajectory of an ion, leaving the blue region of interest temporarily. For a consistent MSD computation, however, the particle is required to stay long enough in the region of interest.

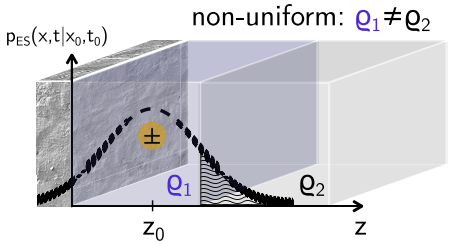

(b) 1D conditional probability density of a particle in the first region close to the interface in z direction, according to Eq. 5, the Einsteinian diffusion equation. If the blue region of interest is constrained using an absorbing boundary condition, the hatched part laying in the adjacent region will never be realised by the particle, and the perpendicular diffusion coefficient is underestimated.

Figure 1: Sketched issues arising from the MSD computation in artificially and non-artificially confined spaces, which may show differing densities ρ.

2.3 Anisotropic Diffusion

In contrast to a pure liquid, particles constituting a liquid in the vicinity of vacuum or a solid, the system is not isotropic any more as previously. The translational symmetry, which is present in a bulk system, is broken in that case. Hence, the diffusion coefficient depends on the coordinate, and needs to be described by an anisotropic diffusion tensor $\mathbf{D}$ (see Eq. 3) with non-diagonal elements [32]. Particle movements may be influenced by varying local densities resulting from interfacial interactions, which is why in general $\mathbf{D}$ depends on the position $\mathbf{r}$. To describe the spatial spread of a probability distribution in such a system with time, one requires the *anisotropic Smoluchowski equation*

$$\frac{\partial}{\partial t} p\left(\mathbf{r}, t|\mathbf{r_0}, t_0\right) = \nabla \mathbf{D} \left[\nabla + \beta \left(\nabla W(z)\right)\right] p\left(\mathbf{r}, t|\mathbf{r_0}, t_0\right) , \tag{8}$$

a modified version of Eq. 2, the Fokker-Planck equation [32]. Here, $p\left(\mathbf{r}, t|\mathbf{r_0}, t_0\right)$ describes the conditional probability distribution function to find a particle at time t at position $\mathbf{r_0}$, under the condition that its initial position was $\mathbf{r}_0$ at time t_0. The density profile $\rho(z) = \rho_0 \exp(-\beta W(z))$ is assumed to be axially symmetric around the z axis, with $\beta = (k_B T)^{-1}$ and $W(z)$ as potential of mean force. Taking into account that $\mathbf{D}$ is diagonal, Eq. 8 can be decomposed. This results in Eq. 4 with D_{xx} and D_{yy} coefficients for x and y components. However, one may not conclude trivially Einstein's diffusion law to hold.

Following the argumentation of Liu *et al.* [32], Eq. 8 can be simplified by manually introducing virtual slabs in the system along the density gradient in z direction. Only if particles stay continuously from time t to $t + \Delta t$ within a virtual slab $\{a, b\}$, they contribute to the mean squared displacement for a specific slab. If the number of particles within each slab does not vary strongly with time, corresponding to the system being in a steady state, it can be shown that Eq. 7, Einstein's diffusion law, suffices indeed to compute diffusion coefficients within slabs in directions *not confined* by boundaries [32]. This is for example true for a simulation using periodic boundary conditions in lateral directions, which is one feature of the systems investigated in this thesis. In the coming section, those systems will be presented together with utilized materials.

3 Materials and Systems

The ionic liquid studied consists of $[C_2Mim]^+$ cations (1-ethyl-3-methylimidazolium) and $[NTf_2]^-$ anions (bis(trifluoromethylsulfonyl)imide). This ionic mixture is known as archetypical model system [30] and has shown desirable physical and chemical properties such as low vapor pressure, high thermal stability, good conductivity and a wide electrochemical window [41], as motivated in Sec. 1. Thus it is a relevant candidate for future industrial applications [42, 43, 44, 45, 46]. In particular, its good solubility of carbon dioxide [47] as well as its application as solvent for the synthesis of ZnO nanoparticles [48] has to be pointed out due to its possible contribution to "green", environmentally friendly chemistry. The chemical structure of the utilized ions is given in Fig. 2. In terms of molecular size, the dimensions are roughly 0.7 nm x 0.3 nm x 0.4 nm for cations and 0.7 nm x 0.4 nm x 0.4 nm for anions, as measured on optimized structures in *VMD* [49], a molecular visualization programme.

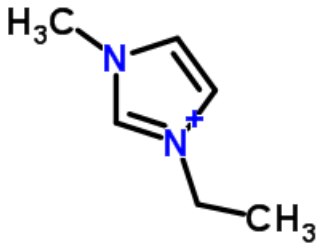

(a) $[C_2Mim]^+$ cation [50]

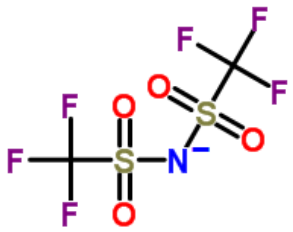

(b) $[NTf_2]^-$ anion [51]

Figure 2: Chemical structures of ions comprising the ionic liquid studied.

In total, four different systems have been studied. Two pure systems with uniform density distributions, consisting of 1,000 water molecules respectively 1,000 ions of each species, were used as references and are shown in Fig. 3. No natural boundaries are embodied here, and particles may move without constraints due to periodic boundary conditions in all directions. The pure systems serve to verify theory as well as computational methods by comparing diffusion coefficients obtained in these systems with literature values.

To investigate systems with non-uniform density distributions, firstly ionic liquid in the vicinity of vacuum with 1,400 ions of each species is studied, depicted in Fig. 4a. Periodic boundaries are applied in all directions in such a way that the liquid is isotropic in x and y directions, but anisotropic in z direction where the liquid forms

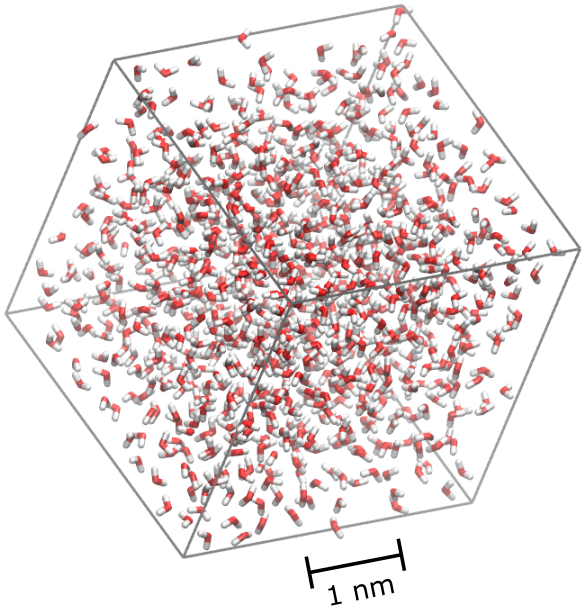

(a) Pure water system. The depicted water molecules reflect their molecular structure, defined by a central oxygen atom (red) and two angled hydrogen atoms (white).

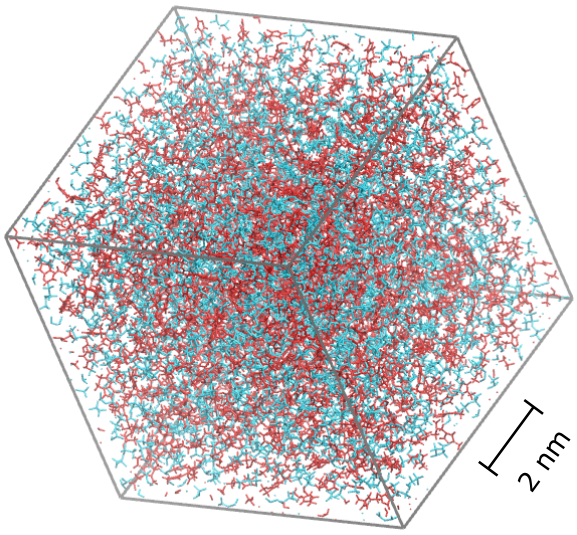

(b) Pure ionic liquid system. $[C_2Mim]^+$ cations are drawn in red and $[NTf_2]^-$ anions in blue.

Figure 3: Orthographic representations of the pure water and pure ionic liquid system using the licorice drawing method.

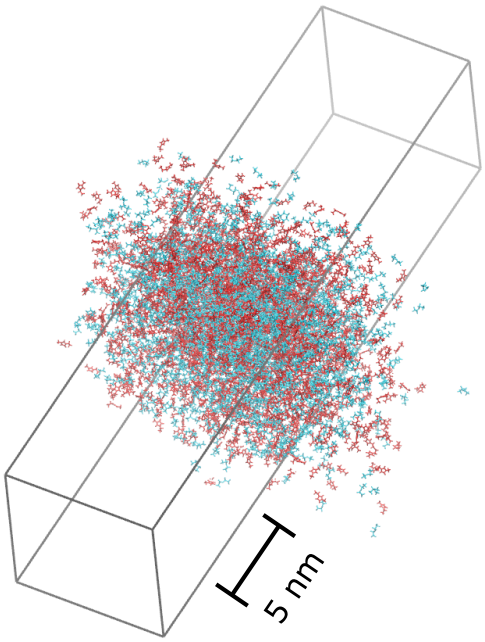

(a) VLV system with unfolded periodic boundaries.

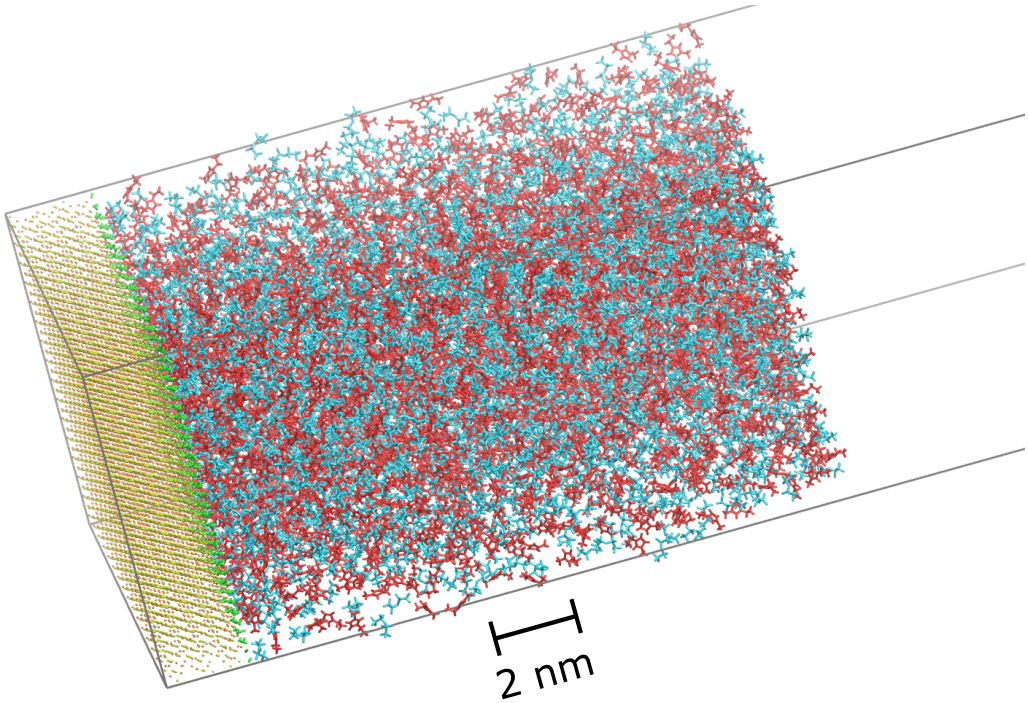

(b) SLV system incorporating a solid, hydroxylated sapphire slab, a slab of ionic liquid, as well as a vast vacuum region. Sapphire is drawn in yellow and orange colours, while green coloured hydroxyl groups are located on top of its surface.

Figure 4: Orthographic representations of the inhomogeneous density systems, vacuum–ionic liquid–vacuum and solid–ionic liquid– vacuum, using the licorice drawing method. $[C_2Mim]^+$ cations are coloured red and $[NTf_2]^-$ anions blue. Scale bars are given to indicate the varying system dimensions.

two interfaces with vacuum.

The main case of interest, a solid–liquid–vacuum system, is sketched in Fig. 4b. It comprises a solid sapphire (Al_2O_3) slab with dimensions 7.57 nm x 6.29 nm x 2.12 nm as well as a fully hydroxylated (0001) x-y surface. In vicinity to it, 1,800 ion pairs were set in a monoclinic simulation box. The hydroxylation implies prevailing negative partial charges located at the oxygen atoms in the hydroxyl groups, which enables hydrogen bonds. For x and y directions, there are periodic boundary conditions, while in z direction movements are naturally restricted by the solid slab and a vast vacuum region respectively. Simulation details can be found in appendix A.1.

4 Methods

4.1 Introducing Virtual Absorbing Boundaries

In an equilibrated, homogeneous bulk system, one would expect the diffusion coefficient D to be constant with time and space, and the density would be distributed uniformly. On the contrary, in inhomogeneous systems with non-uniform density distributions and additional interactions in the vicinity of interfaces, the behaviour of D depends non-trivially on the spatial coordinates.

For cations and anions, different diffusive behaviour must be expected in general for each species due to their different nature. Hence, they must be considered separately in our computations. Furthermore, not every atom of an ion or molecule needs to be tracked to determine its MSD in a certain time interval, but the centre of mass movement suffices. Through analysing these centre of mass movements within regions of interest or *slabs*, discretized MSD values can be obtained, which was set forth in Sec. 2.3. In order to define those regions, it is instructive to look at the density profiles of given systems which are plotted in Fig. 5.
For the bulk systems, density distributions are uniform besides minor, random peaks which may not vanish in bulk regions due to statistical fluctuations. Because of that, slicing may be applied in a uniform way and the z direction is chosen arbitrarily as slicing direction. This results in a certain number of equidistant slabs shown in Fig. 5a–b, in which mean squared displacements are computed. In isotropic bulk systems, the MSD and therefore the diffusion coefficient should not depend on any direction and one would expect the condition $D_{xx} = D_{yy} = D_{zz}$ to hold. Owing to slicing in z direction however, the $D_{zz} = D_\perp$ component will have to be treated with care as it is confined by virtual boundaries, especially in thinly sliced systems, leading to issues explained in Sec. 2.2. For this reason, the MSD in z direction will be recorded separately from the lateral MSD in the x-y plane.

In VLV and SLV systems, non-uniform density distributions are observed, with significant density changes in z direction close to the interfaces. The VLV system shown in Fig. 5c–d reveals an abundance of cations and a shortage of anions close to the vacuum. In the bulk region of the system, the density is approximately constant with only minor fluctuations also seen in the full bulk system.
Fig. 5e–f shows the density distribution of the SLV system along the z coordin-

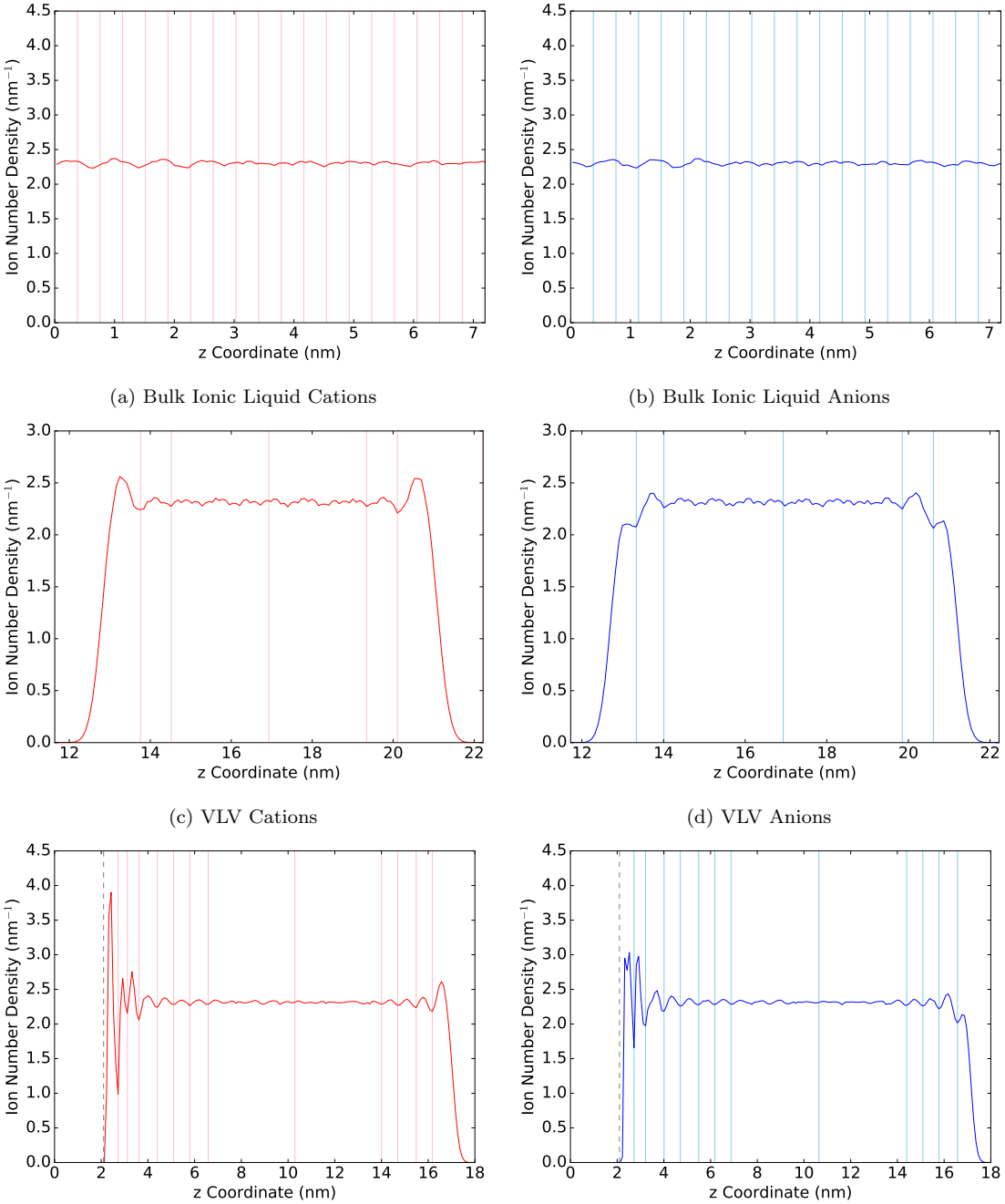

(a) Bulk Ionic Liquid Cations

(b) Bulk Ionic Liquid Anions

(c) VLV Cations

(d) VLV Anions

(e) SLV Cations

(f) SLV Anions

Figure 5: Number densities of each ion species for the pure ionic liquid system, the VLV system and the SLV system. Virtual slab boundaries are plotted with vertical lines. For the pure ionic liquid system an arbitrary number of 20 equidistant slabs is plotted. In sub-figures e and f, the dashed grey line marks the end of the sapphire slab.

ate. Here, close to the solid, both cations and anions have higher abundances, with cations being extraordinarily pronounced. It is followed by a pattern of clearly fluctuating densities, where maxima of cation density at one position are matched quite precisely with minima of anion density and vice versa. This behaviour is evident from the combined density plot for both ion species with higher resolution in Fig. 6. The larger the distance of the liquid from the solid, the lower the peaks become and a vast bulk region is approached. The system has at the other end a vacuum interface, where the same density distributions for cations and anions as in the VLV system can be observed. The latter findings make computing $D_{\parallel}(z)$ particularly interesting for VLV and SLV systems, and slicing them in z direction will yield the desired regions of interest. Studying the density profiles, each major peak could correspond to about one specific molecular layer of ions, and it seems reasonable to study diffusion within these molecular layers. Assuming that one layer is fully characterized by each peak, one may slice the system according to the positions just between two peaks, the minima lying in between them, which can be easily found mathematically. Once the density fluctuations have faded and indistinguishable from statistical fluctuations, two equidistant slabs are introduced in order to validate bulk properties of those regions, until peaks in the region close to the vacuum interfaces appear. There, slicing according to density minima is applied as before. Lastly, when thinking about symmetries in our systems of interest, VLV and SLV systems are both axially symmetric in z direction, taking periodic boundary conditions into account. As a consequence, similarly to the pure system we state $D_{xx} = D_{yy} = D_{\parallel}$ and treat the x and y direction as equal and separate from the MSD computation in z direction.

4.2 Mean Squared Displacement Computation

Having applied appropriate slicing to the system, it is now possible to compute diffusion coefficients with a z resolution dependent on individual slab widths. To do so, particles in each slab are tracked until they leave the slab, while recording their mean squared displacement during a given time interval. Information is extracted from centre of mass trajectories using an custom algorithm and described in the following paragraph. Graphical guidance through the code is provided by the flowchart in Fig. 7.

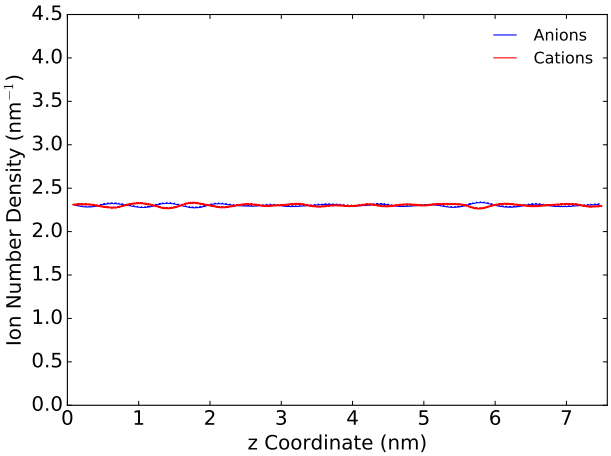

(a) Pure ionic liquid system

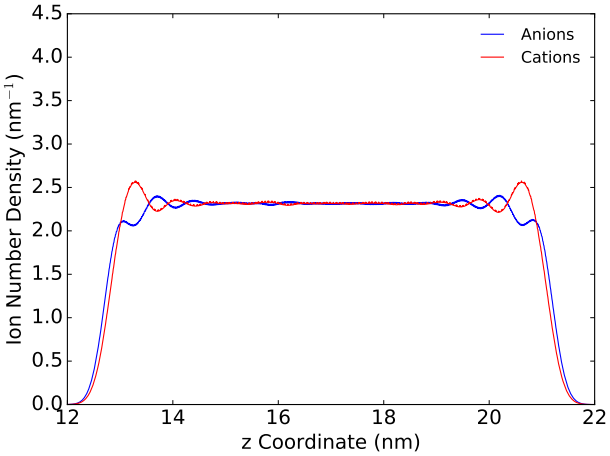

(b) VLV system

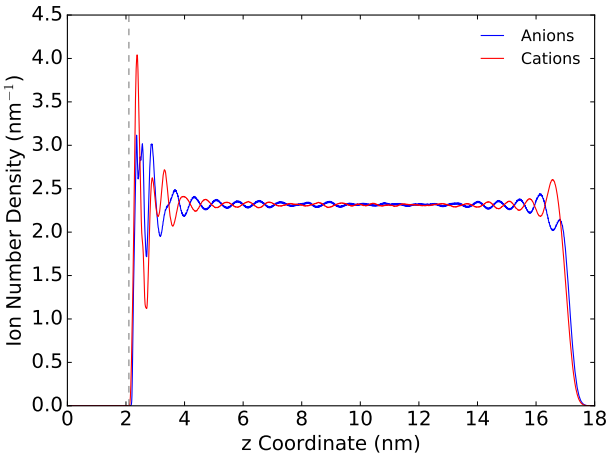

(c) SLV system

Figure 6: Number densities of each ion species, revealing the alternating density extrema between anions and cations. Compared to Fig. 5, these plots were generated with a higher resolution and an averaging procedure.

Firstly, a reference frame at time t_0 is set. The computation of spatial displacements for MSD calculation will refer to coordinates of particles (x_0,y_0,z_0) in this frame. Moreover, all particles are allocated to one specific reference virtual slab or *bin*, dependent on their location within the system. This is done by comparing their z coordinates with the bin boundaries. For bulk systems, periodic boundary conditions in z direction are treated accordingly to ensure proper binning.
Secondly, the subsequent frame at $t = t_0 + t_{step}$ is investigated, where t_{step} may be the smallest time step recorded in the trajectory or in principle any multiple of it. Then, all particles undergo a binning process again based on their new coordinates (x,y,z) at time t. If a change of bin occurred, which is equal to crossing a virtual absorbing boundary, the particle shall not contribute to the MSD in its original bin any more, as it left its specified region of interest. Hence, it will not be considered any more in this *reference* frame iteration. If a particle stayed in the same bin, its MSD is computed as $(x-x_0)^2$, for the x direction, to obtain the MSD for $\Delta t := t-t_0$. Coordinates y and z are treated in the same way. The MSD computed thereby contributes to the sum of all particles in this bin, for this specific displacement time Δt. By simultaneously incrementing the number of sum contributions $N(bnr, \Delta t)$, the average MSD per bin number bnr and displacement time may be computed later on.
Thereafter, a frame step $t := t+t_{step}$ is conducted and the latter iteration – checking whether a particle stayed in its bin and, if true, computing its MSD – is repeated over and over again for frame times $t_0 + n \cdot t_{step}$, until a set endpoint t_{end} is reached. Shifting the current frame may also be terminated when or all particles have left their initial bin.

Then, the reference frame is moved by a certain step, and one sets $t_0 := t_0 + t_{step}$ for instance. From this point on, the above algorithm is performed again until an endpoint or the end of the trajectory is reached for the reference frame. This procedure adds time averages to the ensemble averages, gained by considering multiple centres of masses. Reference frames may be statistically dependent without inducing altering statistical properties as the systems studied may assumed to be ergodic.
Lastly, dividing the MSD sums by the number of sum contributions gives absolute MSD values $\langle x^2 \rangle (bnr, \Delta t)$ – for every coordinate x, y and z. The bin number bnr stands for the centre z position between two successive z bin boundary positions.

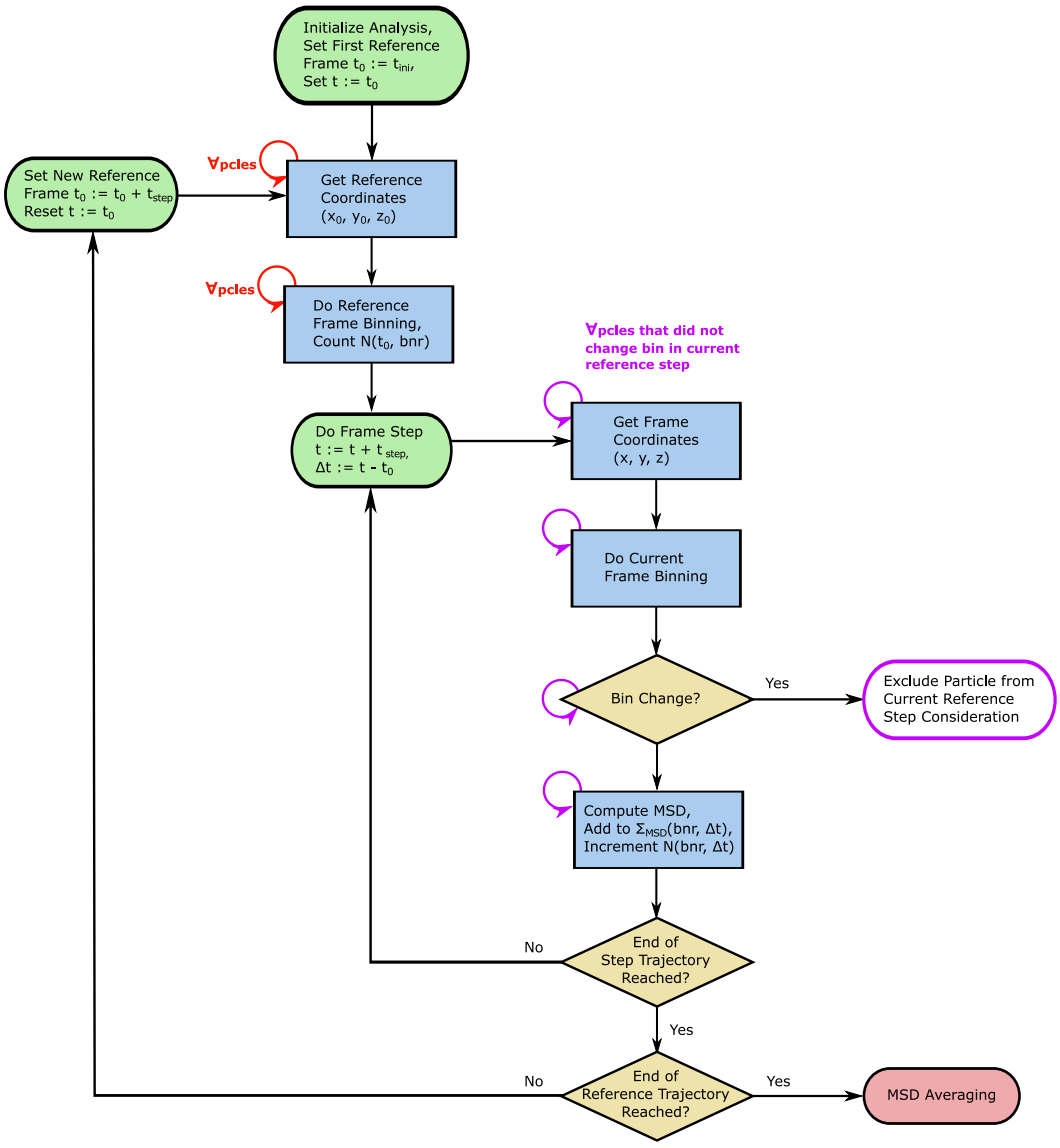

Figure 7: Simplified flow chart for the computation of mean squared displacements from particle trajectories. t_{ini} is the chosen initial time frame from where the trajectory analysis starts, until the last recorded frame is reached. The time that defines the reference frame in the outer loop is t_0, while t is used for current frames in the inner loop. Two consecutive recorded frames in the trajectory differ by the smallest recorded time step t_{step}. The cumulative MSD, Σ_{MSD}, and the number of sum contributions N are realised with multi-dimensional array structures, storing each quantity per bin number and displacement time $\Delta t := t - t_0$. Consult Sec. 4.2 for more information. The result of the algorithm is visualised, for instance, in Fig. 8 for the pure water system.

By plotting computed MSDs over their associated displacement times, one would expect linear growth as predicted by Eq. 7 over a suitable range characterizing the diffusive regime. By fitting a linear function to an appropriate time interval, diffusion coefficients $D(z, \Delta t)$ are obtained as slopes, one for each direction and bin. Choosing fitting intervals is not trivial, however, since time scales matter for diffusive behaviour as explained in Sec. 2.2. Hence, the result strongly depends on the choice of this interval [52].

More information on preprocessing procedures for trajectory analysis, such as computations of centres of mass or number densities, can be found in appendix A.1.

5 Results

In this section, the outcomes of applying the MSD methodology from Sec. 4.2 will be presented and discussed step by step. Recall, that the goal of the MSD algorithm is firstly to compute meaningful diffusion coefficients $D_\parallel$ parallel to virtual slabs, where periodic boundary conditions are given. Secondly, this should demonstrate the failure of this method in constrained directions, here along the z axis, revealing corrupted diffusion coefficients $D_\perp$.
The notation $D^{(n)}$ shall mean the diffusion coefficient for a system sliced in n slabs, and $\overline{D}^{(n)}$ the average diffusion coefficient of all n slabs. An additional index denotes the value of D for the ith slice in an n slab system as $D_i^{(n)}$. In the case of one slab, $D_i^{(1)} = \overline{D}^{(1)} = D^{(1)}$ is known trivially.

5.1 Pure Water System

Let us firstly focus on the pure water reference system, where the last 1 ns of a trajectory with total length 10 ns and a recorded time step of 50 fs were analysed. The evolutions of MSDs with increasing displacement times are depicted in Fig. 8 for various numbers of introduced bins. It can be seen that for displacement times smaller than 0.4 ps, MSDs increase quite fast, with constant slopes, implying fast movements of water molecules at this time scale. The hypothetical short-time diffusion coefficient in the initial regime fitted from 0 ps to 0.4 ps in Fig. 8a is here about 55 % higher than in the long-time regime. In comparison with the characteristic collision time of water, 1 fs to 10 fs, this suggests that we do not observe a ballistic regime, but a different phenomenon.
For times larger than 0.4 ps the slope changes towards a lower value until at least 4 ps for the parallel direction. This is clearly the long-time diffusive regime of interest, where the MSD grows linearly with displacement time for $t \to \infty$. Therefore, fits have been applied from 1 ps to 4 ps to compute diffusivities. Relative least squares fit errors of the slopes $\Delta_{Fit} D_\parallel / D_\parallel$ remain below 0.4% for all numbers of introduced slabs, yielding good fit qualities. An estimate for the standard deviation, resulting from sampling multiple slabs in a system, is given as [53]

$$\sigma_\parallel = \frac{1}{n-1} \sum_{i=1}^{n} \left(D_{\parallel,i}^{(n)} - \overline{D}_\parallel^{(n)} \right)^2 . \tag{9}$$

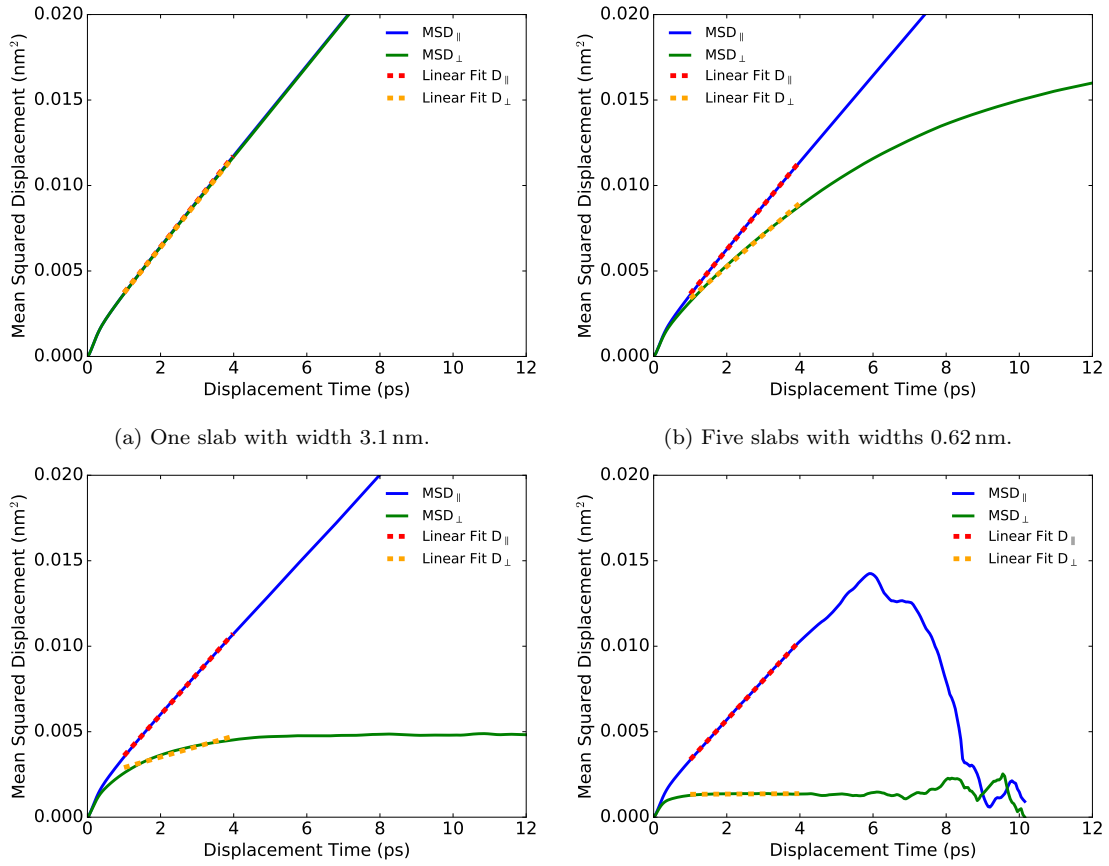

(a) One slab with width 3.1 nm.

(b) Five slabs with widths 0.62 nm.

(c) Ten slabs with widths 0.31nm.

(d) Twenty slabs with widthds 0.16nm.

Figure 8: Mean squared displacements in dependence of displacement time in the pure water system, for various introduced equidistant slab widths. Depicted are results within the first slab of each system. MSDs computed along lateral, not confined directions show a sufficiently linear regime even for small slabs.

For n being twenty, ten and five slabs introduced, the relative standard deviations $\sigma_\parallel / \overline{D}_\parallel^{(n)}$ with reference to the average of D in n slabs, amount to about 8 %, 2 % and 0.5 %, respectively, being relatively small. This confirms bulk behaviour of the systems, as particle movements are almost independent of the slab, and therefore of position, for larger slabs. However, the result for twenty slabs indicates that statistical fluctuations of number densities between slabs may impact computational results in case of thin slabs.

For very large displacement times Δt compared with the initial regime, the curves become unstable and seem to evolve randomly. This is true for all numbers of introduced slabs investigated and for both $D_\parallel$ and $D_\perp$, but can be observed in Fig. 8a–c only for times larger than 12 ps. This phenomenon is likely due to statistics becom-

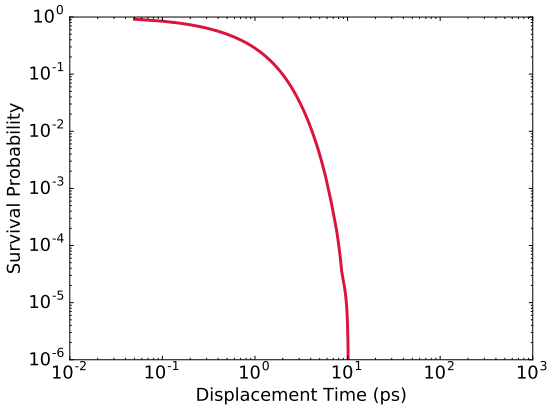

Figure 9: Quickly decaying survival probability for the first slab of the pure water system sliced into twenty slabs with width 0.16 nm each.

ing worse for Δt being much larger than the average residence time of a particle in the slab, as only few particles survive in the slab and contribute to the ensemble average. Fig. 9 supports this hypothesis, depicting the survival probability of one particle staying in the same slab for a certain time. For twenty slabs, corresponding to a slab thickness of 0.16 nm compared with the molecular diameter of water of about 0.3 nm, the survival probability decreases strongly with time passing. It can be observed that just after 0.5 ps, more than 50 % of initial particles left the slab on average and after 6 ps more than 98 % left. No particle survives longer than about 10 ps within this slab. As a result, it is found that with decreasing slice thickness the average residence time decreases, yielding insufficient statistics for ever lower displacement times.

Dependent on the number of introduced slabs, there are strong discrepancies in MSDs for directions parallel and perpendicular to the slicing direction observed. In case of only one slab, where particle movements are only slightly restricted by two boundaries in total, slopes are almost equal for both directions (Fig. 8a). Already with only five introduced slabs (Fig. 8b), the linear regime and the diffusive limit are barely reached for $D_{\perp}$. Eventually, for more than five slabs (Fig. 8c–d), fitting the MSD becomes completely meaningless. The delinearization of the MSD curve is likely the consequence of a curtailed probability distribution due to introduced boundaries, as postulated in Sec. 2.2.

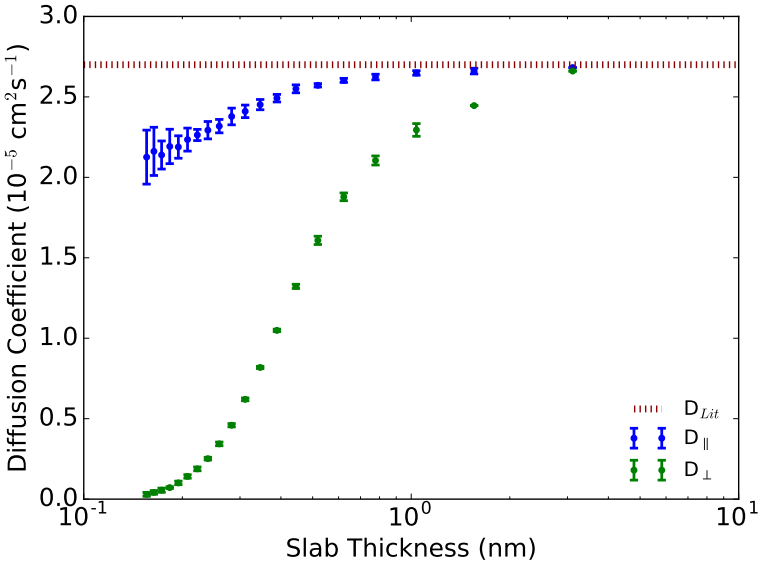

Figure 10: Diffusion coefficients computed as MSDs within virtual slabs, dependent on the number of introduced slabs in the system, for the bulk water system. In each direction parallel and perpendicular, the leftmost point corresponds to twenty and the rightmost point to one introduced virtual slab. Error bars are computed according to Eq. 9. The literature value for the SPC/E model amounts to $D_{Lit} = 2.7 \cdot 10^{-5}\, cm^2 s^{-1}$ [54].

The evolution of computed diffusion coefficients with decreasing slab thickness is visualised in Fig. 10. In case of one single slab, parallel and perpendicular coefficients for only one bin are almost the same, with a relative deviation $|D_{\parallel}^{(1)} - D_{\perp}^{(1)}|/D_{\perp}^{(1)}$ of only 0.8 %. The absolute values are in very good agreement with the literature value of the diffusion coefficient for bulk water in the SPC/E model found by Smith and van Gunsteren, $D_{Lit} = 2.7 \cdot 10^{-5}\, cm^2 s^{-1}$ [54]. Note that Berendsen *et al.*, the creators of the SPC/E parametrization, found a value of $2.5 \cdot 10^{-5}\, cm^2 s^{-1}$ [55].
However, the more slabs are introduced, the more movement in z direction is restricted and $\mathrm{MSD}_{\perp}$ systematically drops with respect to $\mathrm{MSD}_{\parallel}$, resulting in lower diffusion coefficients through lower slopes. Interestingly, not only $D_{\perp}$, but also $D_{\parallel}$ decreases with increasing number of introduced slabs. For twenty slabs, the slab width is only about half the size of the diameter of one water molecule, which could lead to the situation that some fast particles easily leave their slab and do not contribute to the MSD any more. This could result in a bias, where slow particles are given a higher weight in the MSD computation, resulting in lower diffusion coefficients, as observed.
Compared to the literature value, the relative error for water $|D_{Lit} - \overline{D}_{\parallel}^{(20)}|\,/\,D_{Lit}$

for twenty slabs amounts to roughly 22% for water. A tolerance of 5 % is not exceeded, if the number of introduced slabs stays below seven or the slab thickness remains larger than 0.44 nm, being about 1.5 times the diameter of one water molecule. These results imply that modifying the slab width arbitrarily impacts the correct computation of $D_{\parallel}$. Therefore, one will have to take this effect carefully into account, in particular when slicing layered systems according to their density profiles.

Let us summarize the findings of the MSD method for the bulk water system before turning to pure ionic liquid results. Firstly, by reproducing the correct value D_{Lit} for both $D_{\parallel}$ and $D_{\perp}$ in case of one slab, the methodology can be considered as validated. Secondly, the method is not able to compute correct values for $D_{\perp}$ in systems with more than one slab, as postulated. And thirdly, an increase in the number of introduced slabs leads to a decrease of $D_{\parallel}$, probably due to a bias where fast particles are not considered in the MSD computation.

5.2 Pure Ionic Liquid System

In analogy to the bulk water system, the last 30 ns of a 100 ns pure ionic liquid trajectory with a recorded time step with 2 ps were analysed, separately for cations and anions. The MSD behaved in terms of increasing displacement time Δt qualitatively the same compared to the pure water results in Fig. 8. An analogous arrangement of plots is provided in Fig. A.1 in the appendix. For the present system, a fitting range from 150 ps to 300 ps provided a sufficiently linear regime. Qualitatively, $D_{\parallel}$ and $D_{\perp}$ evolve similarly compared to bulk water with decreasing slab thickness, while $D_{\perp}$ decreases here as well with lower slice thickness significantly. Diffusivities of ions shown in Fig. 11 are by roughly two orders of magnitude lower than those of water. Comparing lateral and normal values for only one bin, relative deviations $|D_{\parallel}^{(1)} - D_{\perp}^{(1)}|/D_{\perp}^{(1)}$ amount to 0.3 % for cations and 3 % for anions. Note that there is a difference between analysing trajectories in one bin with two absorbing boundaries, which was done here, and tracking particle in "zero" bins, i.e. without any boundary. The slightly lower value for $D_{\perp}^{(1)}$ for anions might be due to the fact that a small percentage of ions is absorbed to the boundaries, even in the case of a large bin. Absolute values for $D_{\parallel}^{(1)}$ are $3.95 \cdot 10^{-7}\,\mathrm{cm^2 s^{-1}}$ for cations and $2.40 \cdot 10^{-7}\,\mathrm{cm^2 s^{-1}}$ for anions, which will be used as bulk diffusivity references for the VLV and SLV systems.

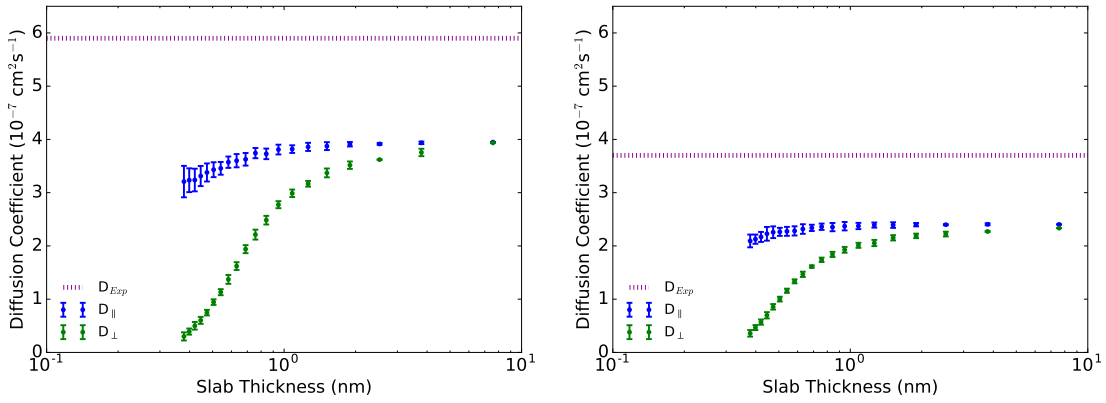

(a) Cations (b) Anions

Figure 11: Diffusion coefficients for lateral and perpendicular directions in bulk ionic liquid for both ion species. Error bars were calculated with the same procedure as used for Fig. 10. Experimental values are $5.9 \cdot 10^{-7}$ cm^{2}s^{-1} for cations and $3.7 \cdot 10^{-7}$ cm^{2}s^{-1} for anions [56].

The value for anions perfectly agrees with the value computed using *GROMACS* MSD computation tools [57], but for cations a small difference amounting to 4 % is found [58]. However, these results pertained to a different analysed trajectory length.

When comparing the two ion species in terms of diffusivities, it can be seen that cations show about 64 % higher diffusion coefficients than anions in case of one slab. Possible reasons for that may be cation–anion attractions, conformational flexibilities, as well as ion sizes and shapes, which are known to influence diffusivities [10].

Comparing $D_\parallel$ results for one bin and twenty bins, relative errors $|\overline{D}_\parallel^{(20)} - D_\parallel^{(1)}| \,/\, D_\parallel^{(1)}$ are 19 % for cations and 13 % for anions. A reason for that deviation could be the same as explained for the water system, namely a bias where slow particles are favoured over fast particles as a result of slicing.

Relative deviations from given experimental values $|D_{Exp} - D_\parallel^{(1)}| \,/\, D_{Exp}$ in case of one slab amount to 32 % for cations and 35 % for anions. These values seem quite high but are still acceptable, as it is known that molecular dynamics simulations using non-polarizable force fields underestimate ionic liquid diffusivities systematically [10].

It was reported that ionic liquids require long simulation times of at least 10 ns before statistically diffusive behaviour could be observed [10]. This is due to ionic liquids reaching their diffusive limit quite slowly. Therefore, varying trajectory lengths ranging from 5 ns to 30 ns were analysed and plotted in Fig. 12. Both

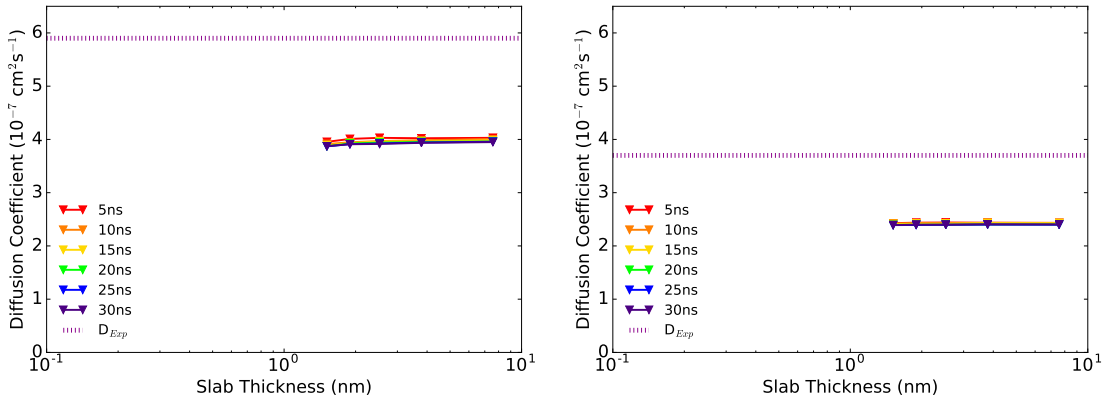

(a) Cations (b) Anions

Figure 12: Lateral diffusion coefficients dependent on trajectory lengths for both ion species as part of bulk ionic liquid. Drawn are sliced systems bearing up to five slices with given slab widths. Respectively, the last 5 ns to 30 ns of a trajectory with a total length of 100 ns were analysed.

ion species reveal very slight decreases in diffusivities with longer trajectories. Maximum relative deviations from the value obtained with a trajectory length of 30 ns, $|D^{(1)}_{\parallel,5ns} - D^{(1)}_{\parallel,30ns}| \,/\, D^{(1)}_{\parallel,30ns}$, are roughly 2 % for cations and 1 % for anions and therefore negligible. This result serves as additional validation of the method, as the same diffusion coefficients were obtained for several trajectory lengths, apart from statistical fluctuations.

5.3 VLV System

Moving on from the pure ionic liquid bulk system, let us examine $D_{\parallel}$ from the last 30 ns of a 100 ns long trajectory of the VLV system with recorded time step 2 ps before eventually reaching the SLV system.

From the density profiles in Fig. 5c–d it can be seen that the outermost layer is more strongly occupied by cations. Similar qualitative results were also found by Smoll *et al.* [59] studying a similar system with an additional cation $[C_{12}Mim]^+$. It is further known that the concentration of alkyl chain carbon atoms of $[C_nMim]^+$ cations is higher at the vacuum interface, which implies the alkyl chain is pointing towards the vacuum [60]. Interestingly, this experimental result has been confirmed by MD simulations in our group when number density was plotted per atom type [58].

Close to the vacuum interfaces it can be seen in Fig. 13 that diffusion coefficients are about 62 % higher for cations and about twice as high for anions, compared to

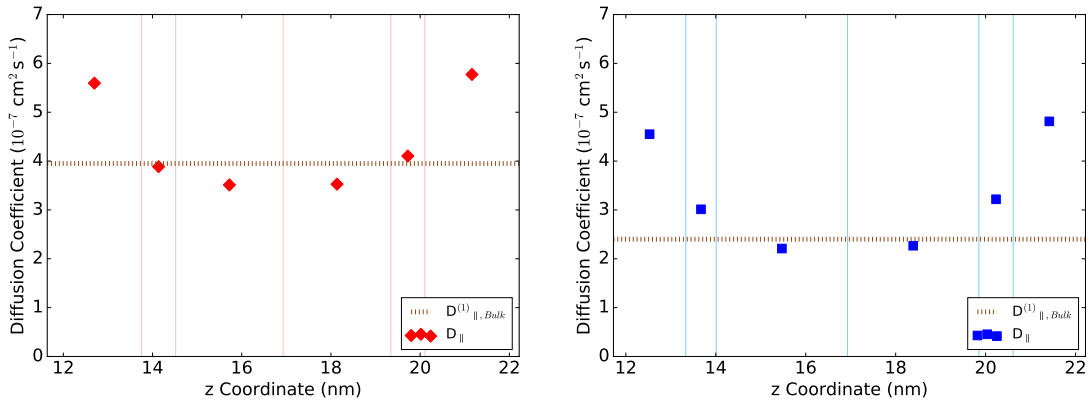

(a) VLV Cations

(b) VLV Anions

Figure 13: Parallel diffusion coefficients for the VLV system for cations and anions. The reference values $3.95 \cdot 10^{-7}\,\mathrm{cm^2 s^{-1}}$ for cations and $2.40 \cdot 10^{-7}\,\mathrm{cm^2 s^{-1}}$ for anions are the computed bulk value within one slab for the pure ionic liquid system, given in Fig. 11.

the bulk value of the liquid in the VLV system, taken as average of the two innermost layers. A higher diffusivity for cations here could be due to the fact that the outermost cation layer at the vacuum interface only interacts with other ions of one parallel adjacent anion layer, while in the bulk there are Coulombic attractions coming from two adjacent layers. Furthermore, less particle collisions reducing ion velocities are expected at the interface.

In the region between the interfacial cation layer and the bulk, Fig. 5c–d conveys that cation density already reached bulk density, while the anion density is increased. This is as well consistent with findings in literature [60]. As far as diffusivities are concerned, $D_\parallel$ is slightly higher than the bulk value in the layers adjacent to the outermost layers for anions, while for cations bulk diffusion is reached, correlating with density observations. Compared to the pure ionic liquid system, the obtained bulk value for $D_\parallel$ in Fig. 13 is here about 11 % lower for cations and 7 % lower for anions than the value computed with the pure ionic liquid system.

5.4 SLV System

Having studied the pure ionic liquid as well as the VLV arrangement, our target SLV system comprising a solid–liquid interface and a liquid–vacuum interface will now be analysed from the solid slab to the vacuum. MSDs were computed from the last 30 ns of a total trajectory length of 100 ns with recorded time step of 2 ps again.

In vicinity of the hydroxylated sapphire slab, cations and anions show number density maxima at the same z coordinates with a difference only in magnitude as plotted in Fig. 6c. This implies, that no electric double layer is being formed, but a different structure. For ionic liquids it was found that double layers are formed if there are both strong ionic correlations and a preference for one ion species on the interface [61], which is true for charged electrodes, for instance. As the surface does not bear any charges, but only partial charges in our system, no preference is found to be given and both cations and anions assemble in the first interfacial layers [30, 58]. Consequently, these layers can be classified as chequerboard-style.

Diffusion coefficients close to the interface are roughly 83 % lower than those meas-

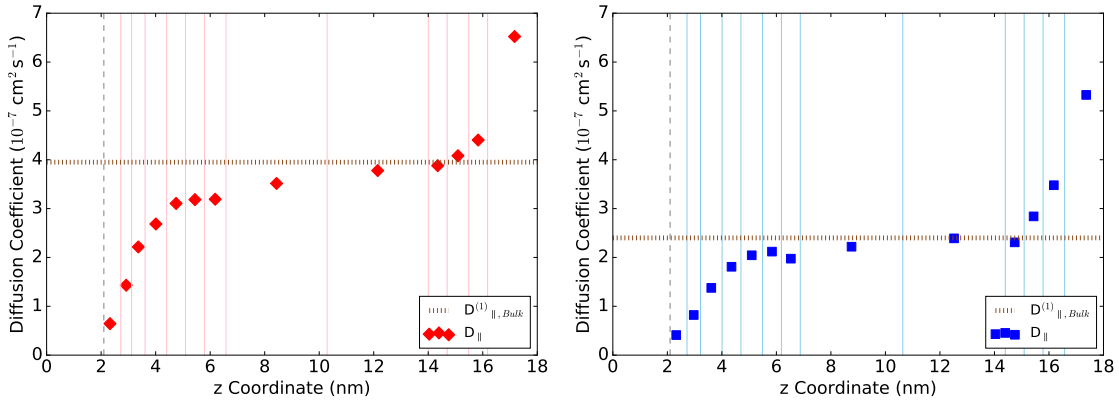

(a) SLV Cations (b) SLV Anions

Figure 14: Parallel diffusion coefficients for the solid–liquid–vacuum system for cations and anions. The reference value $3.95 \cdot 10^{-7}$ cm^{2}s^{-1} for cations and $2.40 \cdot 10^{-7}$ cm^{2}s^{-1} for anions are the computed bulk values within one slab for the bulk ionic liquid system, given in Fig. 11.

ured in the bulk phase, for both ion species, as shown in Fig. 14. This is due to hydrogen bonds between interfacial ions and hydroxyl groups, leading to ion immobilization. Specifically, it was found for this type of system that the imidazolium ring arranges perpendicular to the surface and forms hydrogen bonds with interfacial hydrogen atoms, while the alkyl chain is in a parallel position [30]. For the anion, its oxygen atoms were found to be closest to the surface, forming hydrogen bonds as well. In total, this leads to locked ions at specific positions and therefore explains reduced ion transport.

Adjacent to the first layers, alternating density maxima of cations and anions were found, which asymptotically decrease in magnitude towards a constant bulk value. A similar phenomenon was found by Brkljača *et al.* [30] who studied a solid–liquid–

solid system consisting of the same components as investigated here. Those layered, charge-ordered structures are the result of strong electrostatic interactions [10]. From the interface on, seven regions may be distinguished, until the bulk phase sets in. The larger the distance to the solid slab, the higher the diffusion coefficient becomes and a constant bulk value is – correlating to density observations – reached almost asymptotically. As seen previously in Sec. 5.1 and 5.2, the slab width with respect to molecular size affects indeed the computation of the MSD and therefore impacts the diffusion coefficient. Therefore, the actual value for $D_{\parallel}$ might have to be corrected slightly to a larger value to accommodate for the varying slab widths.

In the bulk phase, slight deviations from the bulk value $D_{\parallel}^{(1)}$ measured in the pure liquid system within one slab are observed, as already found in the VLV system. Deviations of diffusivities in the bulk section closer to the interface, which are slightly lower than the expected bulk value, could stem from a lasting influence of ionic layer-forming interactions even into these distant regions. The second bulk section closer to the vacuum shows a better agreement with $D_{\parallel}^{(1)}$.
In contrast to the solid–liquid interface, close to the vacuum region the diffusivity is about 79 % higher for cations and 130 % for anions compared with bulk in this system. This is a larger increase compared to the vacuum interface in the VLV system in Sec. 5.3, as diffusion coefficients close to vacuum in the SLV system are here about 15 % higher than in the VLV system. In this distant region, the influence of the solid slab should have vanished. Moreover, differing slab widths of the VLV and SLV system close to the vacuum interface might have a smaller impact than elsewhere, as in effect the last system boundary adjacent to the vast vacuum region is not a virtual boundary, but an inherent one, as it is set by the point of zero number density.

To investigate the transport properties of ions within certain layers as well as for checking bulk properties, the SLV system was sliced non-equidistantly according to density minima. This picture may be complemented by equidistant slicing studies shown in Fig. 15. In addition to previous non-equidistant slicing, diffusion coefficient computations within equidistant slabs of 0.7 nm and 0.9 nm thickness were conducted. Separate plots for the equidistant cases are provided in appendix A.2. It becomes clear, that the general trend of diffusivity is captured by all methods. However, there are small deviations coming from different slab widths, which can be seen around $z = 12.3\,\mathrm{nm}$ for example. Three differing values are found at this

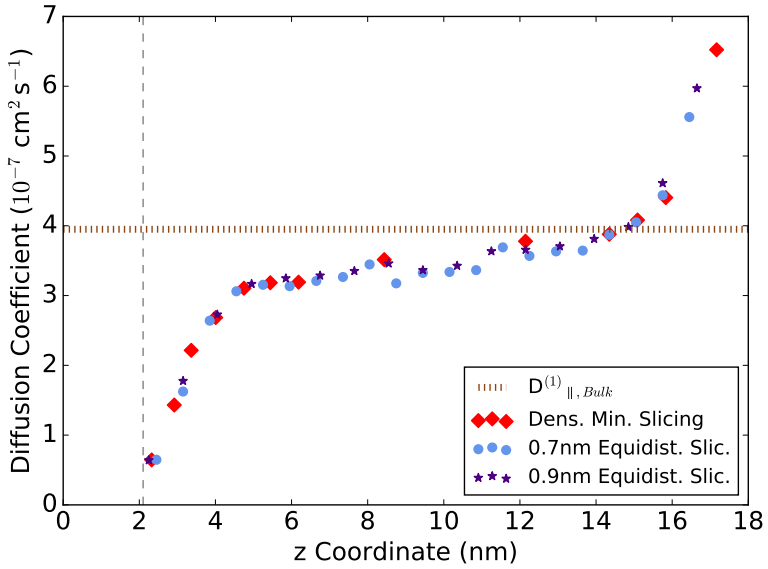

Figure 15: Diffusion coefficients in dependence of z coordinate for the SLV system computed with different slicing methods: according to density minima and equidistant slicing with 0.7 nm as well as 0.9 nm respectively. Detailed plots including slab boundaries can be found in Fig. 14 and Fig. A.2.

coordinate: The diamond represents the large bulk slice and is the highest value amongst those three. For considerably lower slice thickness, represented by the blue dot and the purple star, lower values are found. This underlines the importance of reasonable system slicing once more. For future evaluations, it might therefore be useful to calculate a correction factor based on the deviation for $D_{\parallel}$ in strongly confined regions dependent on the slab thickness in which MSDs are computed. For an even more precise correction, this might require the study of diffusion in a completely unbounded system.

To sum up, through studying diffusion coefficients in the SLV system, the influence of both the solid surface and the vacuum interface on the adjacent ionic liquid has become clear in terms of density and diffusivity, demonstrating the impact of particle interactions on their transport properties.

6 Conclusion

In this thesis, particle trajectories generated through molecular dynamics simulation were analysed in order to compute diffusion coefficients. The target system comprised of a solid slab followed by an archetypical room temperature ionic liquid and a vacuum region. For method validation and consistency checking, reference systems of pure water, pure ionic liquid and a vacuum–liquid–vacuum system were analysed. In essence, the methodology was based on computing mean squared displacements of particles within virtually drawn slabs encompassing regions of interest, with focus on diffusion parallel to the interfacial x-y plane.

Within one slab in the simple pure water system, very good agreement of the computed diffusion coefficients with literature values were obtained for directions both lateral and perpendicular to the x-y plane. In case of more than one slab, the methodology failed – as predicted – when seeking to compute $D_\perp$ along the slicing direction z. This was likely to be due to cutting the edges of the Gaussian transition probability density. However, also the lateral investigation revealed lower diffusion coefficients than the literature value when the slab thickness was too small, which might be due to a bias related to the quick leave of fast particles.
Similar qualitative results relating to the virtual slicing procedure were obtained for the pure ionic liquid system. Cations revealed higher diffusivities than anions. It was further shown that the analysed trajectory length has not a significant impact on the result for trajectories longer than 5 ns.
In the VLV system, cation densities were found to be higher at the vacuum interfaces, making up the outermost layer, as reported in literature. Diffusion coefficients of both ion species were higher close to the vacuum interfaces owing to reduced interactions there.
And lastly, in the SLV system, a 83 % lower lateral diffusion coefficient with respect to the computed bulk value for both ion species is found in the vicinity to the sapphire interface. This underlines the effect of hydrogen bonding between ions and hydroxyl groups, and interactions between cations and anions themselves which stabilize the interfacial structure. Density extrema at the same positions for both ion species in the vicinity to the solid give evidence that the structure is a chequerboard-style layer.

Based on the insights won about diffusion coefficients lateral to interfaces, future analyses of ion trajectories in interfacial systems should focus on the perpendicular component to obtain a full picture of the diffusive landscape at the bulk-interface transition. In the end, these studies will enable a better understanding of interfacial structures and open the door towards technological implementations of ionic liquids.

7 Acknowledgements

Firstly, I would like to thank **Prof. Dr. Ana-Sunčana Smith** for providing me with this interesting research opportunity, supervising my thesis and keeping me calm when deadlines were approaching. I felt always very welcome in her Physics Underlying Life Sciences Group and enjoyed the internationality and kindness. All group members deserve recognition for providing a pleasant social and academic atmosphere.
Furthermore, I am very grateful for having been granted the opportunity by Ana to join the 2018 DPG Spring Meeting and EPS-CMD27 in March 2018 in Berlin. There, I successfully presented a poster about preliminary results of my thesis in the session *Brownian Motion and Transport (Joint session DY/CPP)* [62] and improved my scientific communication skills. I would further like to acknowledge funding for this venture by Friedrich-Alexander University Erlangen-Nürnberg and the Wilhelm and Else Heraeus Foundation.

Secondly, I would like to underline the excellent advisory provided by **Andreas Baer**, reaching from conceptual advise to technical questions such as debugging code. He provided guidance for my Bachelor project – particularly when Ana was pursuing her sabbatical in Australia – and was always there for me, which won him my personal and academic recognition.

Moreover, I would like to thank...
...**Dr. Radha D. Banhatti** for helpful scientific discussions and her general advice for a young scientist,
...**Dr. Robert Blackwell** for his post-doc wisdom, introducing me to the world of Unix and C++, supporting me in devising the MSD algorithm and making use of his `sudo` rights,
...**Nataša Vučemilović-Alagić** for her support with *GROMACS* molecular dynamics simulations and providing ionic liquid trajectories,
...**Robert Stepić** for his chemical knowledge, introducing me to *VMD* and teaching me the Croatian way of life,
...**Oleg Trosman** for cheering me up in hard times by sharing memes with me,
...**Sebastian Ziegler** for fruitful scientific discussions and mental support.

A Appendix

A.1 Computational Details

Trajectories for water and ionic liquid systems utilized in this project were generated using open-source MD software *GROMACS* [63] by PULS group doctoral students Andreas Baer and Nataša Vučemilović-Alagić, respectively, and were subject to further processing by the author. All systems investigated were in a steady state, which was made possible through equilibration and annealing processes. This ensured the ergodicity condition to hold and enabled time averaging, for example.

The water system was devised using the *SPC/E* parametrization [55] ans was firstly subject to a 2 ns equilibration run at 300 K in the NPT ensemble using a Berendsen barostat [64]. In the second run, the system was equilibrated for 5 ns at 300 K in the NPT ensemble as well, but this time with a Parrinello-Rahman barostat [65]. Thirdly, a 5 ns long run in the NVT ensemble was added. These processes were followed by the actual 10 ns long simulation run in the NVT ensemble. More details about simulation parameters may be found in Ref. [66].

One of the first MD simulations and experimental x-ray reflectivity studies for an SLV system consisting of the same components investigated in this thesis were conducted by Brkljača *et al.* [30]. They yielded insights about the quality of fixed-charge force field parametrizations and combining rules. The optimal parametrizations were found to be those of Maginn *et al.* for cations and Canongia Lopes *et al.* for anions [67, 68] with Lorentz-Berthelot combining rules [69, 70]. In this present work, trajectories were obtained by using the above force field parametrizations but with the charge method of *RESP-hf/0.9* (*HF/6–31 g** level of theory) [71]. The solid sapphire slab with its hydroxylated surface was optimized in the *General Utility Lattice Programme* (GULP) [72] and described by the *CLAYFF* [73] force field. In all ionic liquid systems, the starting conformations for the $[NTf_2]^-$ anion were both *cis* and *trans*.
The pure ionic liquid system was firstly minimized followed by a relaxation process using the NVT ensemble for 5 ns and then equilibrated using the NPT ensemble in order to anneal the system for 12 ns. These processes were conducted with a Berendsen barostat [64] and a Nosé-Hoover thermostat [74, 75]. Consequently, 100 ns long particle trajectories were generated at $T = 300$ K with the NVT ensemble.

For the VLV system, the same annealing protocol as for the pure ionic liquid system was executed. The slab of ionic liquid was then provided with about 13 nm wide vacuum regions on each side, giving a total system width of 33.86 nm. This action was followed by a 200 ns long simulation using the NVT ensemble, with a Nosé-Hoover controlled temperature of T = 300 K.
The SLV with its solid sapphire and its adjacent ionic liquid system was minimized and subsequently treated by semi-isotropic NPT annealing for 12 ns as in the pure ionic liquid system. Note that the box size was allowed to vary in z direction in this case. Then, a large vacuum region was set next to the ionic liquid slab, resulting in a total model system width of about 100 nm in z direction. In the last step, a *Langevin algorithm* was utilized to generate 200 ns long trajectories using an NVT ensemble at T = 300 K, followed by an additional 100 ns of simulations with the NVT ensemble at the same constant temperature.
For a detailed description of the ionic liquid simulation procedures, please refer to Ref. [58]. In the end, those simulations yielded positions of every atom for every recorded time frame. This data was further processed to extract information about their diffusive behaviour, which is described in the following paragraph.

Through simulation runs with aforementioned settings, trajectories in the binary *.xtc* format were generated. The first steps to process these trajectories were done using *GROMACS*' `gmx trjconv` tool. All of the following commands are described in detail in the *GROMACS* online reference [76]. To treat periodic boundary conditions of the system, it was ensured that atoms belonging to one molecule were not located across box boundaries using the `-pbc whole` option. Particles that were forced to stay inside the box as they crossed a periodic boundary, were relocated to their real coordinates outside the box using the `-pbc nojump` option. For required group separations into cations and anions, index files were created with the `gmx make_ndx` command. Eventually, the `-com` option of `gmx trjconv` combined with the total number of one ion species given in the `-ng` parameter allowed to compute the centre of mass for each molecule or each ion for every frame in the system.
Number densities of molecules were computed using `gmx density` with the `-dens number` parameter, giving an `.xvg` file as output. For the pure ionic liquid, VLV and SLV systems, 100, 400 and 1,000 slices respectively were specified in the `-sl` parameter for the computation, for each ion species. This lead to rather smooth number density functions depicted in Fig. 5, thus avoiding oversampling or remov-

ing relevant peaks.

Density minima were then precisely found by processing the `.xvg` files using a custom MATLAB script utilizing the `findpeaks` function, obtaining a file containing bin boundaries for each non-uniform system and each ion species. Bulk regions in these systems were further subject to equidistant slicing using a custom Python script.

Precise number density plots with higher resolution in Fig. 6 were generated using about 1,000, 4,500 and 13,000 slices for each ion species in the pure ionic liquid, the VLV and the SLV system respectively.

A.2 Supplementary Figures

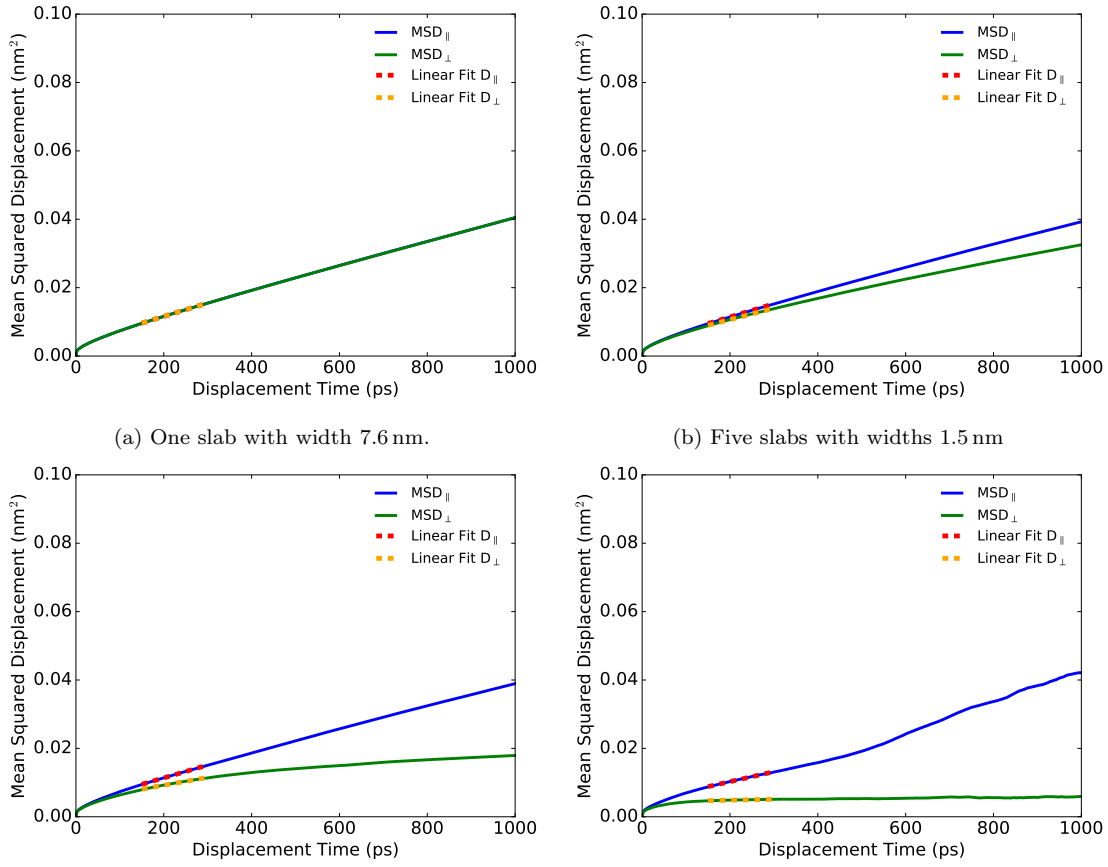

(a) One slab with width 7.6 nm.

(b) Five slabs with widths 1.5 nm

(c) Ten slabs with widths 0.76 nm

(d) Twenty slabs with widthds 0.38 nm

Figure A.1: Mean squared displacements in dependence of displacement time for various introduced equidistant slab widths in the pure ionic liquid system. Depicted are results within the first slab of each system for cations.

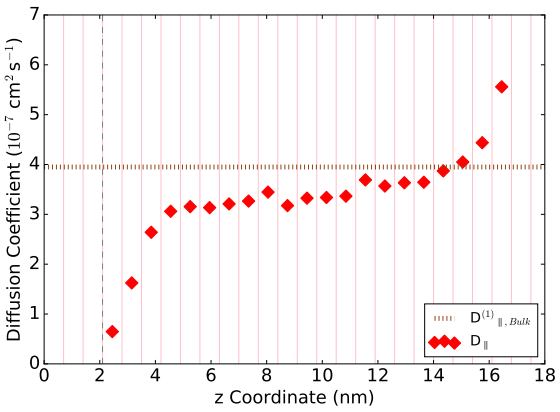

(a) Equidistant slices with a thickness of 0.7 nm.

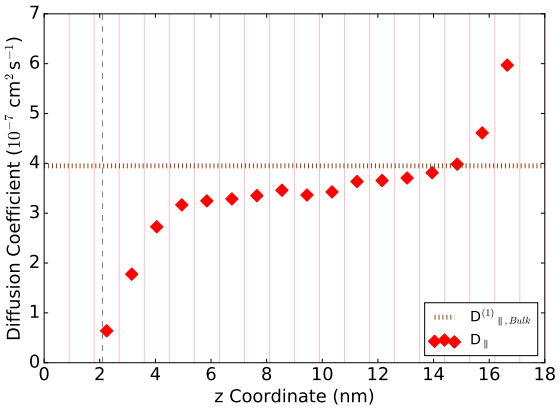

(b) Equidistant slices with a thickness of 0.9 nm.

Figure A.2: Equidistant slicing applied to the SLV system for cations with sketched bin boundaries. Together with the non-equidistant slicing demonstrated in Fig. 14, these sub-figures are summarized in Fig. 15.

References

[1] T. Welton, "Room-Temperature Ionic Liquids. Solvents for Synthesis and Catalysis," *Chemical Reviews*, vol. 99, no. 8, pp. 2071–2084, 1999.

[2] M. Freemantle, "Designer Solvents," *Chemical & Engineering News*, vol. 76, pp. 32–37, mar 1998.

[3] M. V. Fedorov and A. A. Kornyshev, "Ionic liquids at electrified interfaces," *Chemical Reviews*, vol. 114, pp. 2978–3036, mar 2014.

[4] H. Li Chum, V. R. Koch, L. L. Miller, and R. A. Osteryoung, "An Electrochemical Scrutiny of Organometallic Iron Complexes and Hexamethylbenzene in a Room Temperature Molten Salt," *Journal of the American Chemical Society*, vol. 97, pp. 3264–3265, may 1975.

[5] J. S. Wilkes, J. A. Levisky, R. A. Wilson, and C. L. Hussey, "Dialkylimidazolium Chloroaluminate Melts: A New Class of Room-Temperature Ionic Liquids for Electrochemistry, Spectroscopy, and Synthesis," *Inorganic Chemistry*, vol. 21, pp. 1263–1264, mar 1982.

[6] P. Wasserscheid and W. Keim, "Ionic Liquids—New "Solutions" for Transition Metal Catalysis," *Angewandte Chemie International Edition*, vol. 39, pp. 3772–3789, oct 2000.

[7] C. Lagrost, D. Carrié, M. Vaultier, and P. Hapiot, "Reactivities of some electrogenerated organic cation radicals in room-temperature ionic liquids: Toward an alternative to volatile organic solvents?," *Journal of Physical Chemistry A*, vol. 107, no. 5, pp. 745–752, 2003.

[8] K. R. Seddon, "Ionic liquids for clean technology," in *Journal of Chemical Technology and Biotechnology*, vol. 68, pp. 351–356, Wiley-Blackwell, apr 1997.

[9] M. Hayyan, F. S. Mjalli, M. A. Hashim, I. M. AlNashef, and T. X. Mei, "Investigating the electrochemical windows of ionic liquids," *Journal of Industrial and Engineering Chemistry*, vol. 19, pp. 106–112, jan 2013.

[10] S. Tsuzuki, "Factors Controlling the Diffusion of Ions in Ionic Liquids," *ChemPhysChem*, vol. 13, pp. 1664–1670, may 2012.

[11] K. Xu, "Nonaqueous liquid electrolytes for lithium-based rechargeable batteries," *Chemical Reviews*, vol. 104, no. 10, pp. 4303–4417, 2004.

[12] N. Papageorgiou, "The Performance and Stability of Ambient Temperature Molten Salts for Solar Cell Applications," *Journal of The Electrochemical Society*, vol. 143, p. 3099, oct 1996.

[13] J. Fuller, "The Room Temperature Ionic Liquid 1-Ethyl-3-methylimidazolium Tetrafluoroborate: Electrochemical Couples and Physical Properties," *Journal of The Electrochemical Society*, vol. 144, p. 3881, nov 1997.

[14] J. Mun and H. Sim, *Handbook of ionic liquids : properties, applications, and hazards*. Nova Science Publishers, 2012.

[15] E. Van De Ven, A. Chairuna, G. Merle, S. P. Benito, Z. Borneman, and K. Nijmeijer, "Ionic liquid doped polybenzimidazole membranes for high temperature Proton Exchange Membrane fuel cell applications," *Journal of Power Sources*, vol. 222, pp. 202–209, jan 2013.

[16] J. B. Goodenough and K. S. Park, "The Li-ion rechargeable battery: A perspective," *Journal of the American Chemical Society*, vol. 135, pp. 1167–1176, jan 2013.

[17] D. R. Macfarlane, N. Tachikawa, M. Forsyth, J. M. Pringle, P. C. Howlett, G. D. Elliott, J. H. Davis, M. Watanabe, P. Simon, and C. A. Angell, "Energy applications of ionic liquids," *Energy and Environmental Science*, vol. 7, pp. 232–250, dec 2014.

[18] D. Wei and A. Ivaska, "Applications of ionic liquids in electrochemical sensors," *Analytica Chimica Acta*, vol. 607, pp. 126–135, jan 2008.

[19] M. Shahinpoor, Y. Bar-Cohen, J. O. Simpson, and J. Smith, "Ionic polymer-metal composites (IPMCs) as biomimetic sensors, actuators and artificial muscles - A review," *Smart Materials and Structures*, vol. 7, pp. R15–R30, dec 1998.

[20] H. Helmholtz, "Studien über electrische Grenzschichten," *Annalen der Physik*, vol. 243, pp. 337–382, jan 1879.

[21] H. Helmholtz, "Ueber einige Gesetze der Vertheilung elektrischer Ströme in körperlichen Leitern mit Anwendung auf die thierisch-elektrischen Versuche," *Annalen der Physik*, vol. 165, pp. 211–233, jan 1853.

[22] D. L. Chapman, "LI. A contribution to the theory of electrocapillarity," *Philosophical Magazine Series 6*, vol. 25, pp. 475–481, apr 1913.

[23] A. A. Kornyshev, "Double-layer in ionic liquids: Paradigm change?," *Journal of Physical Chemistry B*, vol. 111, no. 20, pp. 5545–5557, 2007.

[24] W. Freyland, *Coulombic Fluids*, vol. 168 of *Springer Series in Solid-State Sciences*. Berlin, Heidelberg: Springer Berlin Heidelberg, 2011.

[25] C. Merlet, B. Rotenberg, P. A. Madden, and M. Salanne, "Computer simulations of ionic liquids at electrochemical interfaces," *Physical Chemistry Chemical Physics*, vol. 15, pp. 15781–15792, sep 2013.

[26] A. Riisager, P. Wasserscheid, R. Van Hal, and R. Fehrmann, "Continuous fixed-bed gas-phase hydroformylation using supported ionic liquid-phase (SILP) Rh catalysts," *Journal of Catalysis*, vol. 219, pp. 452–455, oct 2003.

[27] U. Kernchen, B. Etzold, W. Korth, and A. Jess, "Solid catalyst ionic liquid layer (SCILL) - A new concept to improve selectivity illustrated by hydrogenation of cyclooctadiene," *Chemical Engineering and Technology*, vol. 30, pp. 985–994, aug 2007.

[28] H. P. Steinrück, J. Libuda, P. Wasserscheid, T. Cremer, C. Kolbeck, M. Laurin, F. Maier, M. Sobota, P. S. Schulz, and M. Stark, "Surface science and model catalysis with ionic liquid-modified materials," *Advanced Materials*, vol. 23, pp. 2571–2587, jun 2011.

[29] J. Habasaki and K. L. Ngai, "Heterogeneous dynamics of ionic liquids from molecular dynamics simulations," *The Journal of Chemical Physics*, vol. 129, p. 194501, nov 2008.

[30] Z. Brkljača, M. Klimczak, Z. Miličević, M. Weisser, N. Taccardi, P. Wasserscheid, D. M. Smith, A. Magerl, and A. S. Smith, "Complementary molecular dynamics and x-ray reflectivity study of an imidazolium-based ionic liquid at a neutral sapphire interface," *Journal of Physical Chemistry Letters*, vol. 6, no. 3, pp. 549–555, 2015.

[31] H. J. Berendsen, *Simulating the physical world: Hierarchical modeling from quantum mechanics to fluid dynamics*, vol. 9780521835. Cambridge: Cambridge University Press, 2007.

[32] P. Liu, E. Harder, and B. J. Berne, "On the Calculation of Diffusion Coefficients in Confined Fluids and Interfaces with an Application to the Liquid-Vapor Interface of Water," *The Journal of Physical Chemistry B*, vol. 108, no. 21, pp. 6595–6602, 2004.

[33] A. Einstein, "Über die von der molekularkinetischen Theorie der Wärme geforderte Bewegung von in ruhenden Flüssigkeiten suspendierten Teilchen," *Annalen der Physik*, vol. 322, no. 8, pp. 549–560, 1905.

[34] R. Brown, "XXVII. A brief account of microscopical observations made in the months of June, July and August 1827, on the particles contained in the pollen of plants; and on the general existence of active molecules in organic and inorganic bodies," *Philosophical Magazine Series 2*, vol. 4, no. 21, pp. 161–173, 1828.

[35] Cambridge Academic Content Dictionary, "Cambridge Academic Content Dictionary," 2016.

[36] H. C. Berg, *Random walks in biology*. Princeton University Press, 1993.

[37] P. Nelson, "Biological Physics," *Physics*, vol. 71, no. 2, pp. S419–S430, 2004.

[38] G. A. Pavliotis, *Stochastic Processes and Applications: Diffusion Processes, the Fokker-Planck and Langevin Equations (Texts in Applied Mathematics)*, vol. 60. New York: Springer, 2014.

[39] R. Zwanzig, *Non-Equilibrium Statistical Mechanics*. Oxford: Oxford University Press, 2001.

[40] S. M. Ross, *Introduction to probability models*. Academic Press, 2nd ed., 1980.

[41] Sigma-Aldrich / Merck KGaA, "1-Ethyl-3-methylimidazolium bis(trifluoromethylsulfonyl)imide (Product Information)," *https://www.sigmaaldrich.com/catalog/product/sial/11291 (retrieved 2018-09-14)*, 2018.

[42] S. Corderí, N. Calvar, E. Gómez, and A. Domínguez, "Capacity of ionic liquids [EMim][NTf2] and [EMpy][NTf2] for extraction of toluene from mixtures with alkanes: Comparative study of the effect of the cation," *Fluid Phase Equilibria*, vol. 315, pp. 46–52, feb 2012.

[43] B. Rodríguez-Cabo, A. Soto, and A. Arce, "Desulfurization of fuel-oils with [C2mim][NTf2]: A comparative study," *Journal of Chemical Thermodynamics*, vol. 57, pp. 248–255, feb 2013.

[44] D. Giovanelli, M. C. Buzzeo, N. S. Lawrence, C. Hardacre, K. R. Seddon, and R. G. Compton, "Determination of ammonia based on the electro-oxidation of hydroquinone in dimethylformamide or in the room temperature ionic liquid, 1-ethyl-3-methylimidazolium bis(trifluoromethylsulfonyl)imide," *Talanta*, vol. 62, pp. 904–911, apr 2004.

[45] A. P. Fröba, H. Kremer, and A. Leipertz, "Density, refractive index, interfacial tension, and viscosity of ionic liquids [EMIM][EtSO4], [EMIM][NTf2], [EMIM][N(CN)2], and [OMA][NTf2] in dependence on temperature at atmospheric pressure," *Journal of Physical Chemistry B*, vol. 112, pp. 12420–12430, oct 2008.

[46] S. Handy, ed., *Applications of Ionic Liquids in Science and Technology*. InTech, sep 2011.

[47] A. M. Schilderman, S. Raeissi, and C. J. Peters, "Solubility of carbon dioxide in the ionic liquid 1-ethyl-3-methylimidazolium bis(trifluoromethylsulfonyl)imide," *Fluid Phase Equilibria*, vol. 260, pp. 19–22, oct 2007.

[48] E. K. Goharshadi, Y. Ding, and P. Nancarrow, "Green synthesis of ZnO nanoparticles in a room-temperature ionic liquid 1-ethyl-3-methylimidazolium bis(trifluoromethylsulfonyl)imide," *Journal of Physics and Chemistry of Solids*, vol. 69, pp. 2057–2060, aug 2008.

[49] W. Humphrey, A. Dalke, and K. Schulten, "VMD: Visual molecular dynamics," *Journal of Molecular Graphics*, vol. 14, pp. 33–38, feb 1996.

[50] Royal Society of Chemistry / ChemSpider (adapted), "1-Ethyl-3-methylimidazolium chloride," *http://www.chemspider.com/Chemical-Structure.138894.html (retrieved 2017-12-19)*, 2015.

[51] Royal Society of Chemistry / ChemSpider (adapted), "Bistriflimide," *http://www.chemspider.com/Chemical-Structure.138894.html (retrieved 2017-12-19)*, 2015.

[52] I. C. Bourg and G. Sposito, "Molecular dynamics simulations of the electrical double layer on smectite surfaces contacting concentrated mixed electrolyte (NaCl–CaCl2) solutions," *Journal of Colloid and Interface Science*, vol. 360, no. 2, pp. 701–715, 2011.

[53] W. S. S. Gosset, "The Probable Error of a Mean," *Biometrika*, vol. 6, pp. 1–25, mar 1908.

[54] P. E. Smith and W. F. van Gunsteren, "The viscosity of SPC and SPC/E water at 277 and 300 K," *Chemical Physics Letters*, vol. 215, pp. 315–318, dec 1993.

[55] H. J. Berendsen, J. R. Grigera, and T. P. Straatsma, "The missing term in effective pair potentials," *Journal of Physical Chemistry*, vol. 91, pp. 6269–6271, nov 1987.

[56] H. Tokuda, K. Hayamizu, K. Ishii, M. A. B. H. Susan, and M. Watanabe, "Physicochemical properties and structures of room temperature ionic liquids. 2. variation of alkyl chain length in imidazolium cation," *Journal of Physical Chemistry B*, vol. 109, no. 13, pp. 6103–6110, 2005.

[57] GROMACS Developers, "gmx msd (GROMACS 5.0.7 Manual)," *http://manual.gromacs.org/programs/gmx-msd.html (retrieved 2018-09-24)*, 2018.

[58] N. Vučemilović-Alagić et al., "Manuscript in Preparation (Working Title: Insights from Molecular Dynamics Simulations on Structural Organization and Lateral Diffusion of an Ionic Liquid at Solid and Vacuum Interfaces)." 2018.

[59] E. J. Smoll, M. A. Tesa-Serrate, S. M. Purcell, L. D'Andrea, D. W. Bruce, J. M. Slattery, M. L. Costen, T. K. Minton, and K. G. McKendrick, "Determining the composition of the vacuum-liquid interface in ionic-liquid mixtures," *Faraday Discussions*, vol. 206, pp. 497–522, dec 2018.

[60] K. R. J. Lovelock and P. Licence, *Ionic Liquids Studied at Ultra-High Vacuum*. Hoboken, NJ, USA: John Wiley & Sons, Inc., nov 2012.

[61] M. Mezger, H. Schröder, H. Reichert, S. Schramm, J. S. Okasinski, S. Schöder, V. Honkimäki, M. Deutsch, B. M. Ocko, J. Ralston, M. Rohwerder, M. Stratmann, and H. Dosch, "Molecular layering of fluorinated ionic liquids at a charged sapphire (0001) surface," *Science*, vol. 322, pp. 424–428, oct 2008.

[62] M. U. Gaimann, A. Baer, N. Vučemilović-Alagić, A.-S. Smith, and D. M. Smith, "Application of a Jump-Diffusion Model to Solid-Liquid Interfaces in Ionic Liquids (Poster)," *Verhandlungen der Deutschen Physikalischen Gesellschaft*, vol. IV, no. 53, p. 221 (DY 71.8), 2018.

[63] D. Van Der Spoel, E. Lindahl, B. Hess, G. Groenhof, A. E. Mark, and H. J. Berendsen, "GROMACS: Fast, flexible, and free," *Journal of Computational Chemistry*, vol. 26, pp. 1701–1718, dec 2005.

[64] H. J. Berendsen, J. P. Postma, W. F. Van Gunsteren, A. Dinola, and J. R. Haak, "Molecular dynamics with coupling to an external bath," *The Journal of Chemical Physics*, vol. 81, pp. 3684–3690, oct 1984.

[65] M. Parrinello and A. Rahman, "Polymorphic transitions in single crystals: A new molecular dynamics method," *Journal of Applied Physics*, vol. 52, pp. 7182–7190, dec 1981.

[66] A. Baer, "Relaxation of hydrogen bond network in water subject to an electric field (Master Thesis)," 2017.

[67] M. S. Kelkar and E. J. Maginn, "Effect of temperature and water content on the shear viscosity of the ionic liquid 1-ethyl-3-methylimidazolium bis(trifluoromethanesulfonyl)imide as studied by atomistic simulations," *Journal of Physical Chemistry B*, vol. 111, no. 18, pp. 4867–4876, 2007.

[68] J. N. Canongia Lopes, J. Deschamps, and A. A. H. Pádua, "Modeling Ionic Liquids Using a Systematic All-Atom Force Field," *The Journal of Physical Chemistry B*, vol. 108, no. 30, pp. 11250–11250, 2004.

[69] H. A. Lorentz, "Ueber die Anwendung des Satzes vom Virial in der kinetischen Theorie der Gase," *Annalen der Physik*, vol. 248, no. 1, pp. 127–136, 1881.

[70] D. Berthelot, "Sur le mélange des gaz," *Comptes rendus hebdomadaires des séances de l'Académie des Sciences*, vol. 126, pp. 1703–1855, 1898.

[71] J. P. Hallett and T. Welton, "Room-temperature ionic liquids: Solvents for synthesis and catalysis. 2," *Chemical Reviews*, vol. 111, pp. 3508–3576, may 2011.

[72] J. D. Gale and A. L. Rohl, "The General Utility Lattice Program (GULP)," *Molecular Simulation*, vol. 29, pp. 291–341, may 2003.

[73] R. T. Cygan, J.-J. Liang, and A. G. Kalinichev, "Molecular Models of Hydroxide, Oxyhydroxide, and Clay Phases and the Development of a General Force Field," *The Journal of Physical Chemistry B*, vol. 108, no. 4, pp. 1255–1266, 2004.

[74] W. G. Hoover, "Canonical dynamics: Equilibrium phase-space distributions," *Physical Review A*, vol. 31, pp. 1695–1697, mar 1985.

[75] S. Nosé, "A molecular dynamics method for simulations in the canonical ensemble," *Molecular Physics*, vol. 52, pp. 255–268, jun 1984.

[76] GROMACS Developers, "GROMACS Online Reference Version 5.0.7," *http://manual.gromacs.org/ (retrieved 2018-09-24)*, 2018.

Eigenständigkeitserklärung

Ich versichere, dass ich die Arbeit selbstständig und ohne Benutzung anderer als der angegebenen Quellen angefertigt habe und dass die Arbeit in gleicher oder ähnlicher Form noch keiner anderen Prüfungsbehörde vorgelegt und von dieser als Teil einer Prüfungsleistung angenommen wurde. Alle Ausführungen, die wörtlich oder sinngemäß übernommen wurden, sind als solche gekennzeichnet.

Erlangen, 27. September 2018

_____

Mario Udo Gaimann

Contact

Mario Udo Gaimann

Institut für Theoretische Physik I und
Cluster of Excellence Engineering of Advanced Materials
Nägelsbachstr. 49b
91052 Erlangen
Germany

e: mario.gaimann@gmx.de
m: +49 176 90 75 71 78
w: http://puls.physik.fau.de/